Line Deformations Due To A Planet: A Direct Fitting Approach

Dissertation
zur Erlangung des Doktorgrades
des Fachbereichs Physik
der Universität Hamburg

vorgelegt von

Fabian Pfeifer

aus Groß-Gerau

Hamburg
2013

Gutachter der Dissertation: Prof. Dr. Jürgen H. M. M. Schmitt
Dr. Eike Günther

Gutachter der Disputation: Prof. Dr. Marcus Brüggen
Prof. Dr. Peter H. Hauschildt

Datum der Disputation: 31.01.2014

Vorsitzender des Prüfungsausschusses: Dr. Robert Baade

Vorsitzender des Promotionsausschusses: Prof. Dr. Peter H. Hauschildt

Dekan der MIN Fakultät: Prof. Dr. H. Graener

Abstract

The measurement of accurate orbital elements, in particular the misalignment between the sky projected rotation axis of the host star and the orbit normal of the planet, are important to understand the evolution of planetary systems. During a transit an asymmetric distortion in the line profile shows up, called the Rossiter-McLaughlin-Effect, because of the partial occultation of the rotating stellar disk. As a result, the radial velocity (RV) of the host star shows an anomalous Doppler shift depending on the position of the planet on the disk. Current methods fit this anomalous radial velocity (RV) shift and deduce from it the planetary orbital parameters.

I present in this thesis two different approaches to derive more precise values for the planetary orbital parameters, in comparison to the modeling of the anomaly. Instead of measuring the RV shift, one of my approaches is to directly model the line deformation. The approach is similar to Doppler Imaging used for stellar spot reconstruction. In order to do so a spectral model has been implemented. As a second approach I used a method that has been coined as "Line-Profile Tomographie". By means of Least Squares Deconvolution (LSD) the broadening function of a spectrum is reconstructed for each phase of a transit.

I present a short targets of interest list and will discuss the selection criterion that I have applied. I successfully analyzed data of two systems - HAT-P-2b and WASP-33b - and have promising results for two further systems - WASP-7b and XO-3b.

Simulations and the application to observational data of these systems have shown that the direct modeling depends on the template very sensitively. LSD proved to be widely applicable and stable. The method can indeed be used to improve the precision of two planetary orbital parameters: the misalignment and the inclination of the planetary orbit, in comparison to the modeling of the anomaly.

Zusammenfassung

Die Messung genauer orbitaler Bahnparameter sind, im speziellen die Verkippung der himmelsprojezierten stellaren Rotationsachse des Zentral Sternes zur Bahnnormalen des Planeten, für das Verständnis der Evolution planetarer Systeme bedeutend. Während eines Transits zeigt sich eine asymmetrische Störung, bekannt als Rossiter-McLaughlin-Effekt, hervorgerufen durch eine Teilverdeckung der rotierenden stellaren Scheibe. Daraus folgend zeigt die radial Geschwindigkeit (RV) des zentral Sternes eine anormale Doppler Verschiebung in Abhängigkeit von der Position des Planeten auf der Scheibe. Derzeitige Methoden fitten diese anormale radial Geschwindigkeits-Verschiebung (RV) und folgern daraus die planetaren Orbit Parameter.

Ich präsentiere in dieser Doktorarbeit zwei verschiedene Ansätze zur genaueren Bestimmung der planetaren Orbit Parameter, im Vergleich zur Modulierung der anormalen Doppler-Verschiebung. Anstatt die RV Verschiebung zu messen, ist einer meiner Ansätze die Liniendeformation direkt zu modulieren. Dieser Ansatz ist ähnlich zu Doppler Imaging, welches genutzt wird um stellare Flecken zu rekonstruieren. Zweck dessen wurde ein spektrales Modell implementiert. Der zweite Ansatz basiert auf einer Methode bekannt als “Line-Profile Tomographie”. Durch Anwendung von Least Squares Deconvolution (LSD) wird die Rotationsverbreiterungsfunktion des Spektrums für jede Phase des Transits rekonstruiert. Ich präsentiere ein kurze Kandidaten Liste und diskutiere die benutzten Auswahlkriterien. Erfolgreich habe ich zwei Systeme - HAT-P-2b und WASP-33b - analysiert und vielversprechende Resultate für zwei weitere Systeme - WASP-7b und XO-3b.

Simulationen und die Anwendung auf Beobachtungsdaten dieser Systeme hat gezeigt, dass der direkte modelierungs Ansatz von dem Template stark abhängig ist. LSD zeigte sich als vielseitig anwendbar und stabil. Die Methode kann tatsächlich genutzt werden, um die Genauigkeit der zwei Orbit Parameter, die Verkippung und die Neigung des planetaren Orbits, im Vergleich zu der Modelierung der anormalen Doppler Verschiebung zu verbessern.

Acknowledgements

I hereby thank all the colleagues and friends for their support in the last three years.
I thank my professor Jürgen H. M. M. Schmitt for his support and patience.
I especially thank Stefan and Klaus for always having an open door and for the advice they provided.
I thank my Co-I's Stefan, Klaus, Uwe and Jürgen for supporting me as PI and making it possible.
I thank the guys upstairs and my RTG retreat roommate Holger.
I thank the my colleagues who "suffered" with me at the cafeteria of the hospital every lunch.
I thank my "roommates" Natascha and Uwe for the good working atmosphere and handy comments on different topics.
I thank the members of the RTG 1351 for the possibility to do science and learning interesting stuff.
I thank the staff at the administration for their support especially Angelika.
I thank all the people I forgot to mention (Sorry!).
And at last I a big thanks goes to my parents and my sister for believing in me and for supporting me in whatever I do.

Contents

Chapter 1

Introduction

Since the discovery of the first extra solar-planet (Mayor & Queloz 1995 [37]) a new field of astronomy has attracted scientists, which ranges from detecting extra solar-planets, to planet formation theories, extraterrestrial life etc.. Different methods for the detection of extra solar planets have been developed in recent years, using dynamical effects, microlensing, or photometry. Among the most successful techniques is the "transit method", which requires that the planet transits its star in the line of sight.

To get a better understanding on the statistics and the occurrence of planetary system types different surveys have been done and are still ongoing. One prominent mission for detecting transiting planets has been the KEPLER satellite (one of NASA Discovery missions [40]), launched in 2009. KEPLER was a large step forward and discovered 3602 planetary candidates of which 154 have been confirmed. There are also numerous ground-based programs like for example the WASP project [59] or the HAT-NET [24] project. Counting all missions there is a total number of 1055 confirmed exosolar planets (as of December 16 2013).

Current planet formation theory states that the big gas planets form at large orbital distances, at several astronomical units (au), where the temperature is low enough for the growth of a rocky core that can accrete gas from the protoplanetary disk. In our own solar system the big Jupiter size / Jovian planets have the largest orbits and the smaller earth-size planets are close to the Sun. The discovery of close-in hot Jupiters has shown that this configuration is not common for all planetary systems. There is of course a bias by the fact that our instruments are not sensitive enough for smaller planets (or are just becoming sensitive) and that systems with short periods are easier to spot and confirm than systems that have periods that span more than a couple of days or even years.

It is believed that there is a process that perturbes the system and moves the giant planets inwards, resulting in a wide range of possible orbital configurations. Potential mechanisms could be tidal interaction with the protoplanetary disk, planet-planet scattering or the Kozai effect among others. Each process results in a different final orbital configuration. Tidal interaction for example results in systems that are well aligned. Planet-planet scattering can cause a variety of final orbital configurations with misalignments greater than zero. The misalignment is parametrized by the angle λ, the angle between the sky-projected orbit normal and the stellar spin axis.

There is the indication that if the system has a host star with a temperature above $T_{eff} \approx 6250\ K$ there is a high change that the system will show misalignment (Winn et al. 2001 [64], Schlaufman et al. 2010 [56]). By November 2013 there have been "74 planets with measured spin-orbit alignment published so far, 33 of which show substantial misalignments in at least one publication" to quote Heller [50].

The orientation of the planetary orbit or misalignment can be deduced by modeling the Rossiter-McLaughlin-Effect (Section 1.2, Rossiter 1924 [52] and McLaughlin 1924 [38]). There is a another technique based on the passing of stellar spots which can be applied in exceptional cases, still the Rossiter-McLaughlin-Effect remains the standard measurement method.

The Rossiter-McLaughlin-Effect occurs when a planet transits its host star, which causes an asymmetric distortion of the line profile, due to partial occultation of the rotating stellar disk. This distortion shows up as an anomalous Doppler shift, depending on the position of the planet on the stellar disk, in the measurement of the radial velocity (RV).

In recent years, some attempts have been made to describe this anomalous Doppler shift by means of analytic formulae (Ohta et al. 2005 [44] or Hirano et al. 2011 [27]) and deduce from it the misalignment angle λ. However, the description of the Rossiter-McLaughlin-Effect in terms of a Doppler shift remains an approximation, because actually the line profile is deformed. The deformation manifests in a so called "emission bump" that moves across the line profile during a transit. Therefore, the most appropriate model of the Rossiter-McLaughlin-Effect must take into account the deformation of the line profile explicitly. So, instead of measuring the strength of the anomalous Doppler shift, the approach presented in this thesis is to directly model the line deformation. The aim is an improvement in the accuracy of the determination of the misalignment angle λ. The direct modeling approach has been applied before, e.g., by Collier Cameron et al. 2010 [9] who coined the term "Line Profile Tomographie" to refer to it.

Using spots is based on the fact that if a stellar spot is crossed by the planet the flux reduction due to the planet gets less. A spot is almost dark in regard to the rest of the star. Since the latitude of the spot does not change and if the rotation period of the star is known, the orbit period of the planet is in the range of days, and there are several spots present, the crossing can be used to reconstruct the path of the planetary transit on the stellar disk. The problem with this method is the reliability of the spot coverage reconstruction. The lifetime of a spot is up to a couple of weeks. An error in the coverage results in an error in reconstructed the orbital parameters. There are two authors who independently used this method Nutzman et al. (2011 [41]) and Sanchis-Ojeda et al. (2011 [55]) for the first time.

1.1 Methods For Detecting Planets

In this section I present a brief overview of the most important methods for detecting exosolar planets, that have been developed.

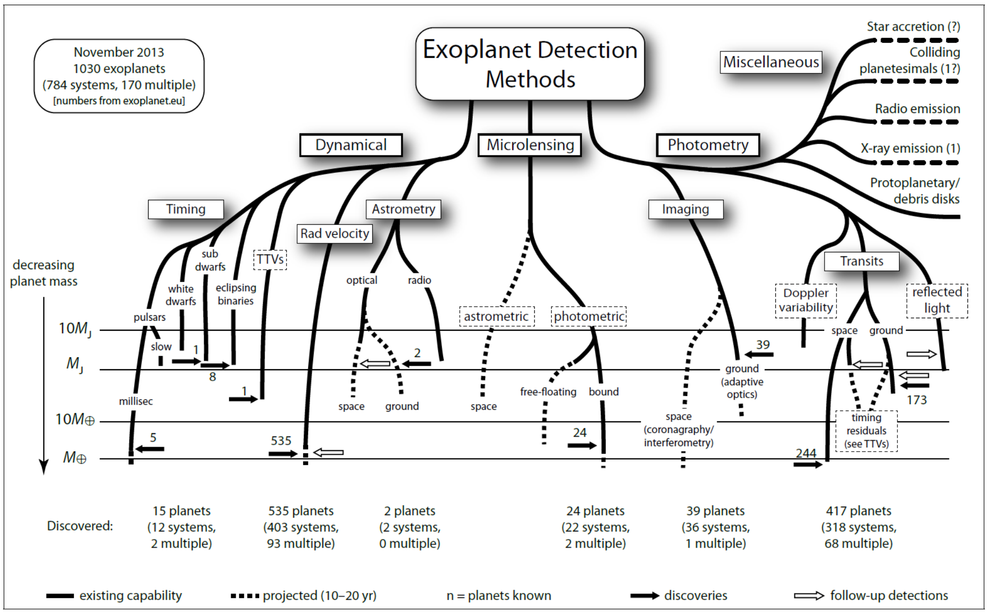

FIGURE 1.1: Visualisation of different planet detection methods and how many exoplanets they discovered / confirmed (figure by Perryman 2013 [46])

Radial Velocity Method Even though in regard to mass, the host star of a planetary system is way more massive, both bodies move around the same center of mass, the barycenter, which is offset to the center of the star. This offset results in a movement of the host star towards and away from the observer which can be measured as a radial velocity (RV) change of the host star. This change in the RV is caused by the Doppler Effect. The method is limited by the number of spectral lines, the rotation velocity of the host star, and a stable instrument is needed which can achieve the required accuracy. For small planets detections the value is below 1 m/s. If the host has a fast rotation rate the line profile is shallow, shows blends and any shift will be hard to detect. Also if the host star is massive, which is the case for early-type stars, a more massive planet is needed to produce a detectable RV signal. Other limits are the brightness of the host and the activity which introduces a RV jitter to the final solution.

It is possible to detect multiple planets in a system with this method. RV measurements are also needed as a follow up to a transit detection, to rule out false positives. The transit method, as described below, relies on a flux reduction during a transit. There are several other phenomena in stars that can cause such a reduction like activity, spots, background eclipsing binaries or grazing transits in binary systems, therefore an independent RV measurement is needed as confirmation. The advantage of the RV method is that it can detect planets that do not transit in the line of sight of the observer. RV measurements are usually done with ground based telescopes. Most of the currently known planets have been detected using this method. A downside of this method is that even though it is possible to get orbital parameters (eccentricity, semi mayor axis) the planet itself cannot be characterized in any detail. The only parameter that can be derived is a lower limit for the planetary mass (msini). In particular, the inclination of the planetary orbit cannot be determined with this method.

Transit Method This method relies on the fact that the planet transits its host star in the line of sight in regard to the observer. The probability for a transit is:

$$P(transit) = \frac{R_{star}}{a} \tag{1.1}$$

where a is the value of the semi-mayor axis of the planetary orbit.

During a transit a reduction in the flux of the host star can be observed since the planet is in comparison to its host star black and has a negligible temperature. Multiple transits have to be observed to confirm the periodicity of the flux reduction. The transit method has the disadvantage that the flux reduction could also stem from stellar variability or spots, the system could be a binary or a transit of a main-sequence star in front of a giant star. To ensure that the system is not a binary the secondary transit has to be analyzed and to confirm that there is really a planet a second measurement with the RV method has to be conducted. Fig. 1.2 shows a typical transit light curve. The curved shape is caused by limb darkening.

The drop in brightness due to the transit in the line of sight is (without accounting for limb darkening):

$$\frac{\Delta I}{I} \approx \left(\frac{R_{planet}}{R_{star}}\right)^2 . \tag{1.2}$$

Therefore as for the RV method there is a bias towards large close in planets as the flux reduction is then more pronounced and a smaller semi-mayor axis results in a higher transit probability and significant shorter orbital period.

A method for the detection of additional planets in a system is the Transit Timing Variations (TTV) method. If more than one object is in an orbit around a star, variations in the mid-transit times indicates to the presence of an additional body(s), a perturber. The variation depends on the masses and orbits of the objects involved. With this method potentially even Earth size planets can be detected.

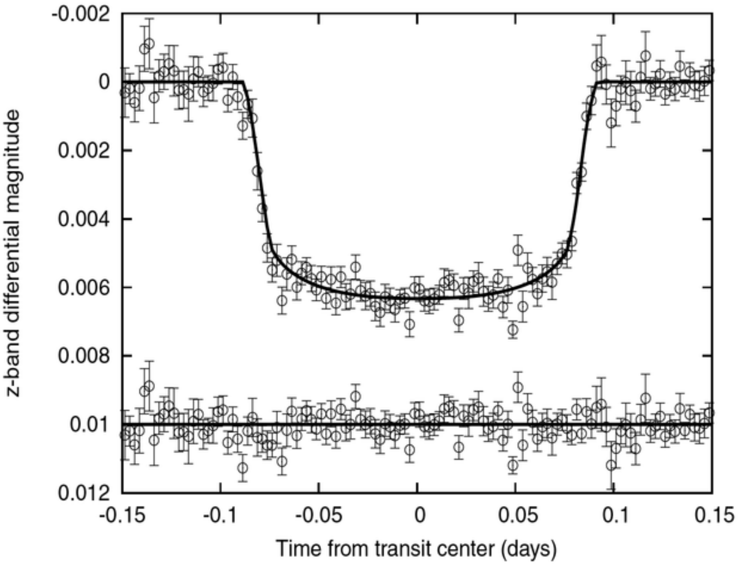

Figure 1.2: Transit light curve of HAT-P-2b by Pál et al. 2010 [45]. The data consists of seven transit events that have been folded and binned.

1.2 Rossiter McLaughlin Effect

In our own solar system the planets are not strongly misaligned in regard to the rotational axis of the Sun. To be able to assess if alignment is more common then misalignment a way to measure the alignment of a planetary system is needed.

One currently used method to measure the misalignment is the Rossiter-McLaughlin-Effect (Rossiter 1924 [52] and McLaughlin 1924 [38]).

Bands parallel to the stellar rotational axis have a constant radial velocity in regard to an observer (assuming rigid rotation) and result in different Doppler shifts for each region. In a prograde orbital configuration, the planet transits first the blue shifted part of the stellar surface. This results in an apparent red shift of the spectrum. When crossing the rotation axis of the star into the red shifted part of the stellar surface this results in an apparent blue shift of the spectra. When measuring the resulting shift over time a typical RV curve is produced (Fig. 1.3). The velocity is defined as positive when moving away from an observer (red) and negative when moving towards an observer (blue). A prograde orbit means that the planet orbits in the same, and a retrograde orbit means that the planet orbits in the opposite direction as the stellar rotation.

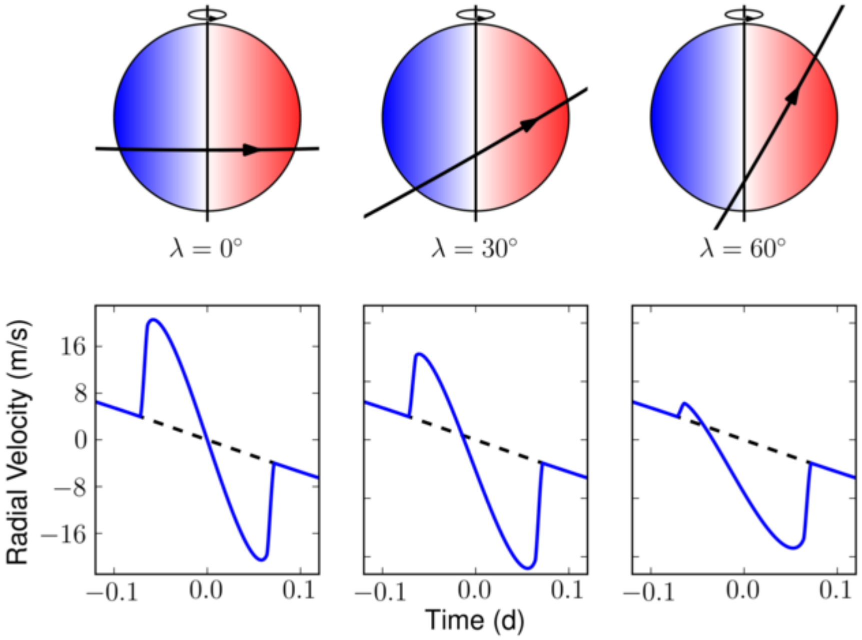

FIGURE 1.3: Three different simulations showing the Rossiter-McLaughlin-Effect for different orbit / spin misalignments. At the top it is shown how the planet transits its host star. At the bottom the solid lines were calculated by using Ohta et al. analytic formulae and the dashed show the RV change due to the motion of the star caused by the planet. For all three the same planetary orbital inclination value $i = 85°$ was used. For the other parameters e.g. the radius of the planet no values from a real system were used but reasonable values were chosen (planet / star size ratio of 0.05).

The Rossiter-McLaughlin-Effect is depending on the following properties of the system:

1. The sky projected equatorial velocity of the host star
2. The inclination of the planetary orbit
3. The projected misalignment angle λ between the orbital plane and the stellar spin axis
4. The size ratio of the planet and host star

There are two methods for obtaining a RV curve: cross correlation and the iodine cell method. Both methods need also some non transit data points to get a orbital solution for the stellar motion which has to be corrected for. When subtracted at the phase position of the transit only the anomaly remains. The RV anomaly can then be fitted by a model to obtain the planetary orbital parameters.

Cross Correlation Cross Correlation is a technique that is used to measure Doppler shifts in astronomy. There have been several approaches to study the properties of this technique and estimate its precision. Early works include Simkin 1974 [57], Davis et al. 1978 [12] and Tonry et al. 1979 [60]. Zucker 2003 [68] presents an approach that includes the possibility to obtain an error estimation. I used the formulae presented in his paper for a cross-correlation to compute the presence of a RV shift later in this thesis (Section 4.2.2).

In the following I do a simplified description of the workings of the method, but in principle this is the idea behind a cross-correlation. For cross-correlation first of all a stellar template is needed. Shifting the template bin-wise multiplying it with the observed spectrum and plotting the respective sums results in a line profile that has a Gaussian shape. There can be deformation caused by not accounting for the barycentric motion around the sun. Also the point spread function (PSF) of the spectrograph has to be accounted for. In a next step a Gaussian or higher order polynomial can be fitted to this profile. If a deformation is present in the line profile this has the effect that the maximum of the Gaussian or polynomial is shifted away from zero. The best match of the template and the observed spectra represents the value of the RV shift. For example plotting this shift against time results in the characteristically shaped RV curve that shows a non-zero amplitude in case of a transiting exosolar planet (Fig. 1.3). This RV curve can then be fitted with a model and the orbital parameters can be extracted.

Iodine Cell Method The Iodine cell method is based, as the name implies, on the use of an Iodine absorption cell that is placed in the path of light in front of the spectrograph. The extra lines provide a wavelength scale and can be used to measure the RV shift present by modeling the observed spectra. The algorithm behind this is described by Butler et al. 1996 [4] and I will give a short summary of the workings of the method in the following.

The basic principle is described by this formulae (Eq. 1 of Butler et al.):

$$I_{Obs} = k[T_{I2}(\lambda) I_S(\lambda + \Delta\lambda)] * PSF \ . \tag{1.3}$$

The stellar intrinsic spectrum I_S is a template spectrum which has been interpolated to the wavelength range of the observation I_{Obs} and k is a scaling factor for the normalization. It is then multiplied by the transmission function of the Iodine cell T_{I2} and convolved with the point spread function of the spectrograph (PSF). Through the adjustment of $\Delta\lambda$ the value of the Doppler shift $z = \Delta\lambda/\lambda$ can be recovered.

Analytic Approaches There have been several approaches in the recent years to model the RV anomaly through analytic formulae. Queloz et al. 2000 [49] were the first to measure the Rossiter-McLaughlin-Effect for an exosolar planetary system and to attempt a numerical description of the strength of the radial velocity anomaly caused by the planetary transit.

A direct analytic modeling that uses the first moment of the line profile was done by

Ohta et al. 2005 [44] and Giménez et al. 2006 [19] that, incorporating orbit parameters, can recover the misalignment angle λ from the anomaly. The first moment is the intensity-weighted mean wavelength. The advantage of this is that the modeling does not depend on the intrinsic line profile.

Both models have the problem that the RV measured for an observed system are obtained using either the cross-correlation or the Iodine cell method. Hirano et al. 2010 [26] showed that the formulae by Ohta et al. show deviations for large and more rapidly rotating stars in comparison to the result from cross-correlation. This can be fixed by calibrating each system numerically and by calculating the correlation of the strength of the anomaly and the position and size of the planet.

Instead of doing these numerical studies Hirano et al. 2011 [27] extended the modeling with a semi-analytical approach to include macroturbulence and the instrumental profile. These effects have besides the stellar rotation an influence on the observed RV anomaly and broaden the line profile. In their analysis using mock data they show that the anomaly is indeed dependent on the PSF but the macroturbulence has a minor effect on the final result.

In any case, the approach by Hirano et al. remains an attempt to mask a more fundamental problem: the characterization of a profile deformation by a radial velocity shift. In this thesis I will completely circumvent this deficiency and present a more appropriate treatment of the problem based on directly modeling the line profile deformation caused by the planetary transit.

Chapter 2

Line-Profile Reconstruction Techniques

In this chapter a description of the two approaches used in this thesis, the **Direct Profile Modeling** (DPM) and **Least Squares Deconvolution** (LSD), to determine the inclination angle i and the misalignment angle λ of a transiting planet's orbit is given. Simulations using real system parameters were done, in order to quantify the potential of each method to recover input values, and to get an estimate on the error budget.

The simulated systems include HAT-P-2 and WASP-33. One reason for not only simulating one system, but two is that HAT-P-2b is in a highly eccentric orbit, whereas WASP-33b is in a circular orbit around its host star. This makes it possible to test the feasibility of extending the fit, by not only fitting the inclination angle i and the misalignment angle λ, but also other orbital parameters such as the eccentricity. Both planet hosting stars also exhibit a different rotation velocity with a value of 86.02 ± 0.06 km/s (Collier Cameron et al. 2010 [10]) in the case of WASP-33 and 21.3 ± 1.3 km/s (Loeillet et al. [35]) in case of HAT-P-2. The value of 20 km/s is widely considered to be the lower velocity limit where Doppler Imaging[1] is possible.

The main reason for doing two simulations is that part of this theses covers an analysis of observations of both planet hosting stars (Chapter 4).

2.1 Direct Profile Modeling

Theory: During a transit an asymmetric distortion in the line profile shows up, as a result of the partial occultation of the rotating stellar disk by the planetary shadow. As a result, the radial velocity (RV) of the host star shows an apparent anomalous

---

[1] Doppler Imaging is the term used for techniques that reconstruct the spot coverage of a stellar surface, from deformations of spectral line profiles (Vogt, Penrod 1983 [63])

Doppler shift depending on the position of the planet on the disk. Current methods fit this apparent anomalous radial velocity (RV) shift - the so called Rossiter-McLaughlin-Effect - and deduce from it the planetary orbital parameters (see Section 1.2). Since the planetary transit does not cause a real RV shift [2] of the spectra during the transit, this is only an approximation. Instead of measuring this apparent RV shift, one approach of this thesis is to directly model the line deformation caused by the planetary shadow on the stellar disk. In order to quantify the accuracy of the direct profile modeling method, a code has been developed which describes the influence of the planet at any time during a transit.

In the model the definition of the planet's position in time is based on a Keplerian orbit. The Keplerian orbit has to be solved numerically, since there is no way to calculate the distance between the star and the planet as a function of time analytically, the so called "Keplerian Problem" (see e.g. C. D. Murray et al. 2011 [39] for derivation of the solution). According to the Keplerian first law of orbital motion, the radius r of the orbit is (Fig. 2.1(a)):

$$r = \frac{a(1-e^2)}{1+ecos(f)} \ . \tag{2.1}$$

If the eccentricity e is zero the planet moves in a circular orbit around its host star and the radius r is equal to the semi-mayor axis a. For eccentricities larger then zero the radius r reaches a minimum for $a(1-e)$ the point of periastron passage, the point of closest approach of planet and host star. A maximum for r is reached for $a(1+e)$ the point of apastron passage. The value of f is the true anomaly with $f = \theta + \bar{\omega}$. The angle $\bar{\omega}$ is the so called argument of periastron passage, the angle between the radius vector r and the periapse. The angle θ is called the true longitude. The orbit in three dimensions can then be described as (Fig. 2.1(b)):

$$\begin{aligned} X &= r(\cos\Omega\cos(w+f) - \sin\Omega\sin(w+f)\cos I) \\ Y &= r(\sin\Omega\cos(w+f) - \cos\Omega\sin(w+f)\sin I) \\ Z &= r\sin(w+f)\sin I \ . \end{aligned} \tag{2.2}$$

Here the stellar rotation axis is in the Y-axis, Z points towards the observer. When the planet orbit inclination is 90° the orbit is in the X-Z plane. The inclination, I, of the planetary orbit is not to be confused with the inclination of the stellar rotation axis. The longitude of the ascending node is Ω, in my case it has the same value as the misalignment angle λ. The angle λ is the sky projected angle between the stellar rotation axis and the orbital plane of the planet. Finally the argument of periapse is ω with $\bar{\omega} = \Omega + \omega$.

Whether a transit is observable depends on the inclination. Values different from 90°

---

[2] not to be confused with the barycentric motion of the host star due to the planetary transit that does cause a real RV shift of the spectra.

shorten the transit duration. A special case is when the angle for the inclination and λ are 90° which results in a transit along the rotation axis of the host star. The RV curve is in this case flat since the rotation of the stellar surface below the planet is zero in regard to the observer. The planetary "bump" remains in the absorption line center and does not move across the profile.

(a) A ellipse based on the radius of Eq. (2.1). The value of a stands for the semi-major and b the semi-minor axis. The eccentricy is e and the longitude of periastron passage is $\bar{\omega}$. The argument of periapse is ω and f is called the true anomaly

(b) A visualization of the Keplerian orbit according to Eq. (2.2).

FIGURE 2.1: A visualization of a Keplerian planetary orbit.

The Planetary Model In the model, the stellar line profile can be a rotationally broadened Gaussian, a more realistic one, such as a PHOENIX [25] spectrum or any other given stellar template. The deformation caused by the planetary shadow during the transit is represented by a so called planetary template. The planet's template, a scaled non-broadened stellar template, is Doppler shifted according to the radial velocity of the stellar surface below the planet's center. The two scaling factors are the limb darkening factor and the size ratio of the planet and its host star at the given time of the transit. Using the position of the planet's center on the stellar disk to determine the limb darkening factor and the RV shift, is a **small planet approximation**, which assumes that the area covered by the planetary shadow does not show a large gradient for the radial velocity and the limb darkening coefficient.

The following steps are needed for the model:

1. A non-broadened stellar template
2. A rotationally broadened stellar template
3. The limb darkening factor below the planets center at any given time
4. The radial velocity below the planets center at any given time
5. The fraction of the stellar disk covered by the planetary shadow at any given time during the transit

6. Subtracting the Doppler shifted scaled "planetary" template from the broadened "stellar" template

The rotational broadening function is given by (according to D.F. Gray [21]):

$$G(\Delta\lambda) = \frac{2(1-\epsilon)[1-(v_z/v_L)^2]^{1/2} + \frac{1}{2}\pi\epsilon[1-(v_z/v_L)^2]}{\pi v_L(1-\epsilon/3)}. \tag{2.3}$$

The value ϵ is the linear limb darkening coefficient of the host star. The velocity v_L stands for the rotational velocity of the host star, vsini, and v_z is the velocity shift from the line center.

> **Limb darkening** is caused by the fact that the light we observe is emitted by the photosphere which has different layers of temperature and density. Both temperature and density decline for an increasing distance to the stellar center. The light an observer "sees" depends on the optical depth which defines when the thickness of an absorbing gas makes the star become opaque. At the edge of a star an observer cannot "see" as deep into the star as at the center. This darkens the limb of a star.

The linear limb darkening law reads:

$$\frac{I_c^0}{I_c} = 1 - \epsilon(1 - cos(\nu)) \tag{2.4}$$

where ϵ is a coefficient between zero (no limb darkening) and one, and ν is the angle between the surface normal and the line of sight. Here, $1 - cos(\nu)$ can then be substituted by the following expression:

$$\frac{I_c^0}{I_c} = 1 - \epsilon(1 - (X^2 - Z^2)/r_{star}^2) \tag{2.5}$$

where X and Z are the values from Eq. (2.2), I_c is the continuum intensity and I_c^0 is the intensity at the center of the stellar disk. This value is one of the scaling factors which determines the impact of the planetary template in the spectral model.
The value of the RV shift is determined using the Keplerian orbit to calculate the position of the planetary shadow on the stellar disk. Additionally, during ingress and egress, the values for the limb darkening factor and the RV shift have been fixed to not exceed the minimum / maximum values possible. Ingress and egress stand for the phase of the transit at which the planetary disk is still not completely on top of the star and the phase when the planetary disk starts to leave the stellar surface. The error introduced through this has been explored and it was decided that it is negligible for my purposes (Fig. 2.2,Fig. 2.3 and Fig. 2.4) since I focus on stars with rotation rates

above 20 km/s. During ingress and egress the planetary signal is even less pronounced in comparison to the noise level of the spectra, so any approach that tries to model this part of a transit directly will have problems fitting the signal in a correct way, which will result in large uncertainties.

To determine the stellar surface area covered by the planet's shadow $\lambda^e(p,z)$ the formula by K. Mandel and E. Agol 2002 [36] is used and the scaling factor is chosen accordingly:

$$\lambda^e(p,z) = \begin{cases} 0 & 1+p<z \\ \frac{1}{\pi}[p^2 k_0 + k_1 - \sqrt{\frac{4z^2-(1+z^2-p^2)^2}{4}}] & 1-p<z\leq 1+p \\ p^2 & z \leq 1-p \\ 1 & z\leq p-1. \end{cases} \tag{2.6}$$

The value of $p = r_{planet}/r_{star}$ is the size ratio of the planet and its host star, and $z = d/r_{star}$ is the normalized distance between the centers, and the two substitutions are $k_0 = cos^{-1}[(p^2+z^2-1)/2pz]$ and $k_1 = cos^{-1}[(1-p^2+z^2)/2z]$. When the first condition is met, the stellar and planetary disks are completely detached, a configuration that I will call "off star" in the following. The second condition covers the ingress and egress phase of the transit. The third and forth are met when the planets shadow is completely attached to the stellar disk. The forth condition would result in a planet that has the same size or is larger then its host star when viewed from an observer on Earth. The last two configurations will be called "on star" in the following. To simplify the problem a circular stellar disk is assumed and any deformation, like flattening caused by stellar rotation, is neglected.

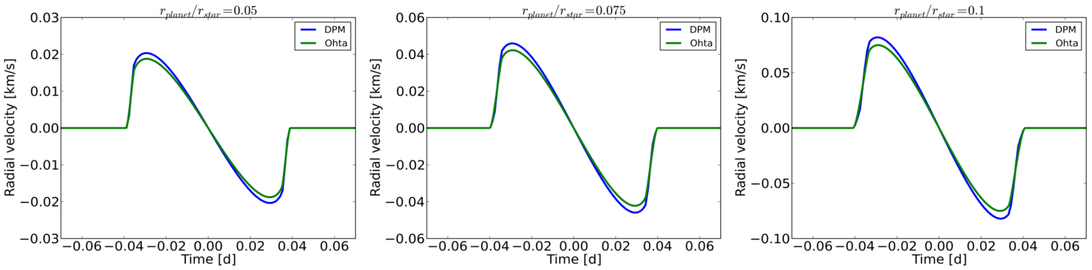

FIGURE 2.2: Rossiter-McLaughlin RV curve for a stellar rotation velocity of 10km/s for different planet / star size ratios.

Testing the model The resulting code was used to produce synthetic transit spectra using literature system parameters of WASP-33 and HAT-P-2 (Table 2.1) with a PHOENIX [25] line profile as stellar template, a S/N ratio of 100, a bin size of 0.05 Å and a wavelength range of 500 Å. To to be comparable the phase information of the

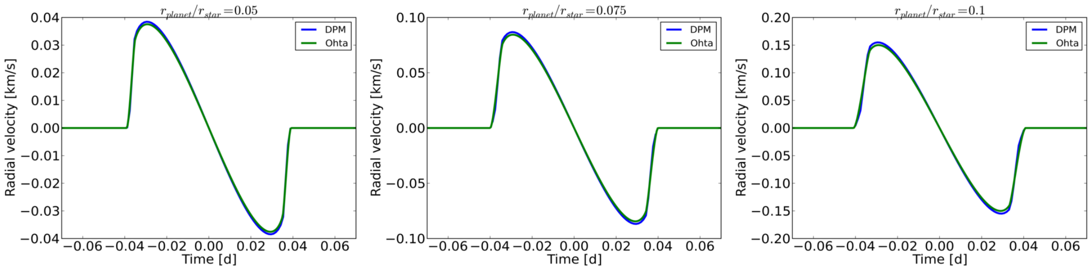

FIGURE 2.3: Rossiter-McLaughlin RV curve for a stellar rotation velocity of 20km/s for different planet / star size ratios.

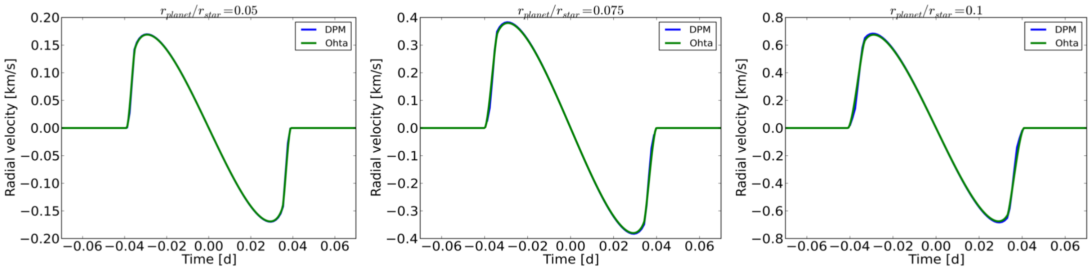

FIGURE 2.4: Rossiter-McLaughlin RV curve for a stellar rotation velocity of 90km/s for different planet / star size ratios.

real transit data was used. This way it can be tested how accurately the method can recover known input values. In the case of HAT-P-2b for the misalignment angle λ a value of 10° was chosen, and for the inclination a value of 92°, which are both within the error margins of the literature value of zero and 90°.

First tests were carried out using the PHOENIX stellar line profile as template for the fit. As a prove of concept, for each of the transit phases, a set of possible planet positions were calculated, varying only the misalignment angle λ and inclination angle i of the planetary orbit (without noise). These data were then used as the "model" to calculate reduced χ^2 values with the noisy data set, and the result plotted as a color map with the orbital inclination angle i and the misalignment angle λ as y- and x-axis, respectively. Varying only the inclination and λ, results in extremely low error bars that are, at first glance, below any reasonable value. The data consists of many data points and there are only two free fit parameters. A possibility is that the low errors are a the result of giving the code the correct phase positions. At each phase, to be able to fit the bump of the planetary signal correctly, the code may have only a narrow range of possible values for the inclination and λ.

To investigate the **influence of the phase** information on the results, the literature value for the one sigma orbit period error were used to calculate a new set of phase values. To increase the effect of the error, the phase was calculated for a transit happening 1000 transits after the literature T0. Even though it is small over time the

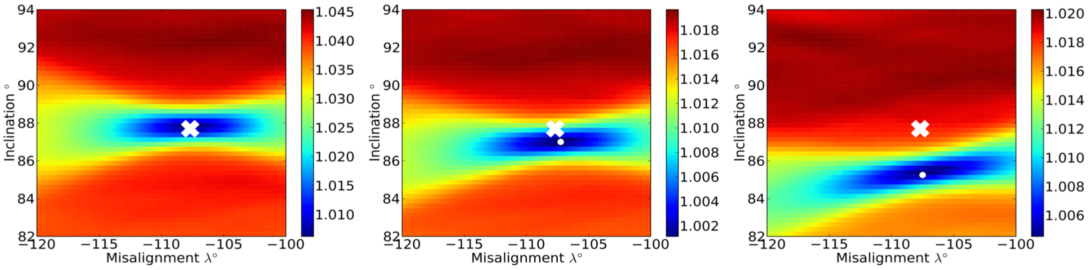

FIGURE 2.5: Exploring the influence of the period on the determination of planetary orbit parameters using WASP-33b literature values. From left to right: zero, five and 15 sigma error on the period (1000 orbits since T0). The white cross marks the literature values and the white point the lowest χ^2 value.

error adds up. Using unrealistic values of a 5, 10, 15 and 20 sigma error on the period, the calculation resulted in values for the inclination that are off in regard to the input values but for λ the values are within two bins of the input values (Fig. 2.5). In my sampling one bin is 0.25°. To conclude: for the orbit geometry of the WASP-33 system the error on the rotation period (i.e. the phase) has no influence on the determination of the misalignment angle λ of the system. At this point of the investigation the simulation has shown that the method works and is able to recover the orbital input parameters.

> There are various sources that can cause an **error in the determination of the inclination**. The inclination has direct influence on the duration of the transit. The planetary signal is weak during ingress and egress due to limb darkening and the reduced area covered by the planet. Therefore for the ingress and egress phases it is hard to fit the transit correctly using the direct profile modeling approach, which results in a apparently shorter transit. Combining this with the error that stems from the error on the phase information the inclination is prone to an unknown level of error. This has to be kept in mind when comparing literature values for the inclination, especially if the transit duration is known from light curve analysis.

Since it is almost impossible to get a perfectly fitting template for a real data set, in a next step a more realistic approach for fitting the simulated data sets was used. There are many effects that cause deformations in a line profile (e.g. an imperfect wavelength solution, instrumental effects, the normalization, etc.) and a model is fitted which can hardly be perfect (not accounting for all physical effects, missing lines, etc.). Instead of using the PHOENIX template for the fit, the same approach was chosen that was used for the real data sets. To obtain a template the SPECTRUM code by Gray was used to get a line list to carry out a multi-Gaussian fit to the simulation. I refer the reader to Section 3.3.4 for a detailed description on the workings of the method.

To further investigate the capability of the model to recover input parameters, and to be able to estimate the error, not only reduced χ^2 maps were calculated but also a Monte Carlo Markov Chain (MCMC) fit was done to the WASP-33b / HAT-P-2b transit test spectra respectively, using 50,000 steps. For both simulations the inclination angle i and the misalignment angle λ were set as free fit parameters.

As shown in Fig. 2.6 in the case of WASP-33 the quality of the fit degrades in comparison to the one that uses the PHOENIX template. The lowest value for the reduced χ^2 is for inclination values that result in a non-transiting system. Around the input values there is a area of low reduced χ^2 values. That the reduced χ^2 is not close to one, results from the fact that some lines are missing in the line list and for strong deep lines the fit with a Gaussian does not work. This is just a cosmetic effect since it introduces an offset but does not influence the position of the lowest reduced χ^2 value. For the HAT-P-2 system the fit does recover values for the orbital inclination i and the misalignment angle λ that are, without any doubt, completely wrong and impossible to achieve based on the input values (Fig. 2.7). The much higher value for the reduced χ^2 values in the map also indicate that the goodness of the template fit is worse than the one for the WASP-33 simulation. This can be the cause of more missing lines, which for the simulation is not a problem. The simulations, even though this is less realistic since both stars have a differing spectral classification, use the same PHOENIX template and the same line list. Both simulations differ in the rotation velocity of the host start, the linear limb darkening factor ϵ, the size ratio of the host star and the planet, the orbital parameters and the random noise that has been applied to the simulation. It was further investigated if increasing the vsini to higher values (40 and 90 km/s), using a larger wavelength range (1000 Å) or enlarging the planet by a factor of 1.5, would result in a better agreement with input values for HAT-P-2. All these tests did not improve the result.

The reason for the direct fit to fail is uncertain. If it is the combination of system parameters or a single parameter that causes the failure is, as of today, unknown. The only explanation that can point in the right direction is that as soon as an imperfect template is used the fit starts failing in recovering the input parameters. The lower reduced χ^2 values for the WASP-33 simulation also point in this direction (better fitting template).

As mentioned above a MCMC fit was carried out using the same transit code as for the simulation. As the reduced χ^2 map has shown the code is able to recover the input values for the WASP-33 system. There is an offset of about one degree in the inclination and the misalignment angle λ but the input values are within the 95% credibility interval. For the HAT-P-2 system simulation the same MCMC fit was done. As the reduced χ^2 map had shown it is not possible to recover the correct input values for

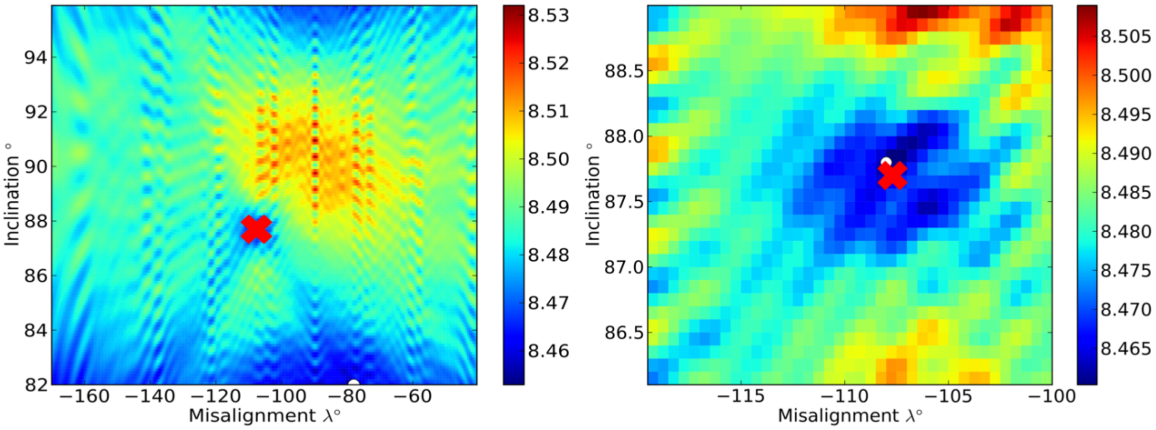

FIGURE 2.6: Reduced χ^2 maps calculated using WASP-33 literature system parameters (Table 2.1). On the right a zoom in on the location of the input values. The white dot marks the lowest reduced χ^2 value in the maps. The red cross marks the input values of the simulation.

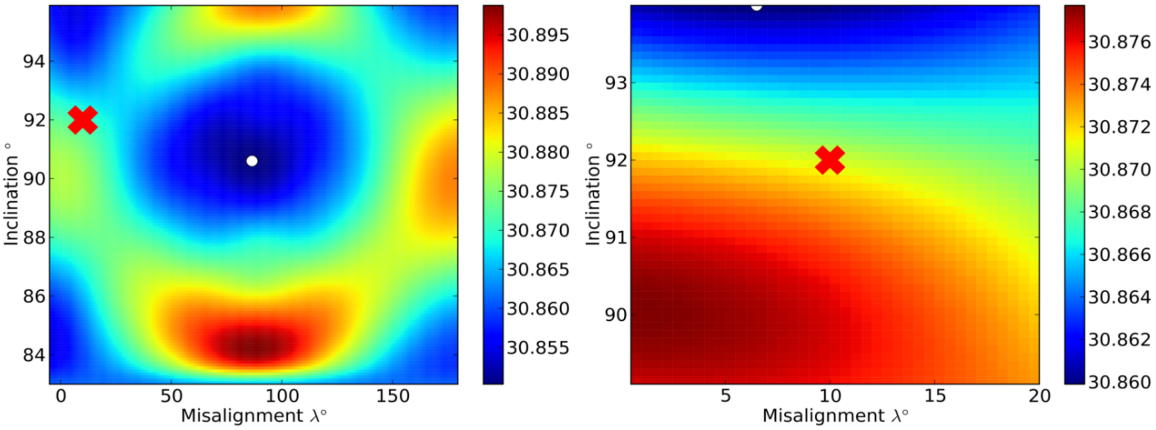

FIGURE 2.7: Reduced χ^2 maps calculated using HAT-P-2 literature system parameters (Table 2.1). On the right a zoom in on the location of the input values. The white dot marks the lowest reduced χ^2 value in the maps. The red cross marks the input values of the simulation.

the orbit. This is therefore also true for the MCMC fit. Since the reduced χ^2 map for the HAT-P-2 simulation already showed that it is impossible to recover the input values no further calculations using more than 50000 steps were done. I also considered it unreasonable to include the eccentricity and the argument of periastron in the model.

I also did an investigation of the influence of two effects on the resulting output values: phase smearing and the wavelength dependence of the rotational broadening.
To calculate the orbital position of the planet during a transit, the code will use the time information provided in the header of the spectra of observational data. Observational data has a nonzero exposure time which results in **phase smearing** since the planet moves during an exposure. In the model only the mid-time between the start and the

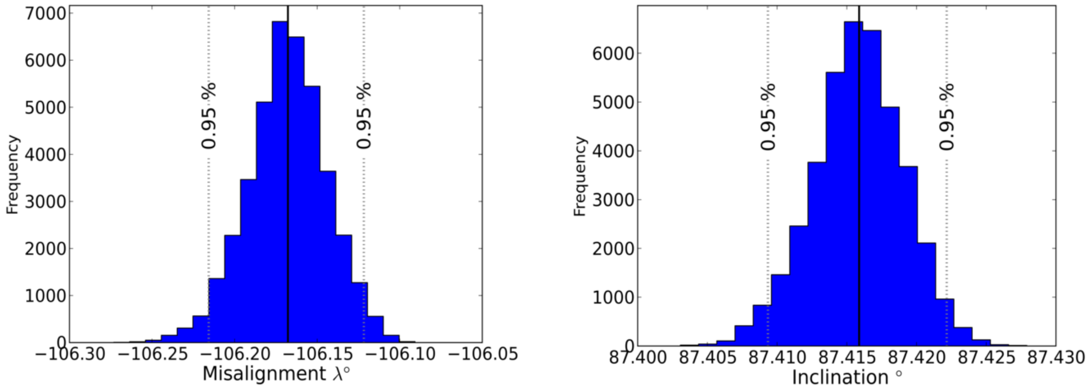

Figure 2.8: Frequency histograms for the inclination and the misalignment of the MCMC calculation done for the WASP-33 transit simulation.

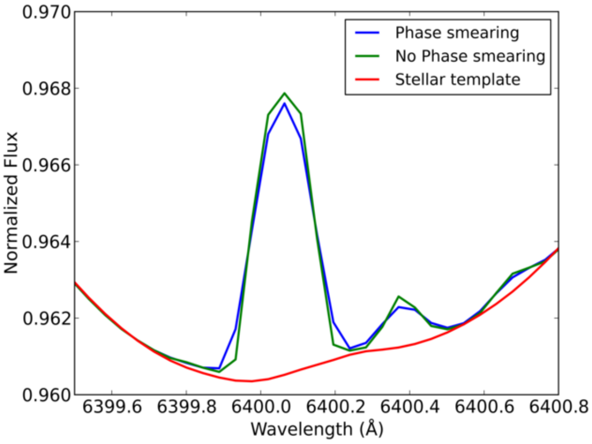

Figure 2.9: The influence of phase smearing due to non-zero exposure times on the line profile deformation due to a planetary transit. The phase smearing was simulated using the mean of 11 data points.

end of the exposure is used as phase information. Therefore the planet is not moving during each “exposure”. To simulate phase smearing, 11 transit points were calculated for each exposure and then their mean was taken, using the spectral resolution of a real data set. Using more then 11 transit points does not change the form of the final profile in any noticeable way for an assumed exposure time of 600 seconds. This can differ for lower or higher exposure times. As Fig. 2.9 shows the influence of phase smearing can be neglected.

The **wavelength dependence** of the **Doppler shift**, causes the rotational broadening of a spectrum to be wavelength dependent. The model does not account for this, for computation time reasons. Even though for small wavelength regions this effect should be rather small, the deformation caused by a planetary transit signal is also relatively weak, depending on the star/planet size ratio. I verified that the effect is not of the same magnitude as a planetary signal (Fig. 2.10) and can be neglected for wavelength ranges of 100 Å (when fitting a template to observational data I used chunks with a length of 80Å).

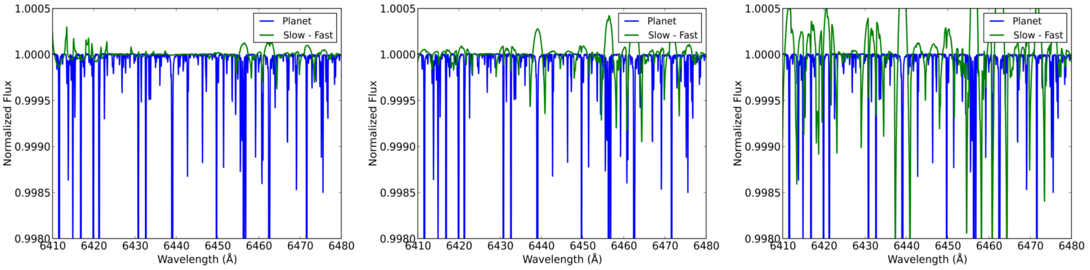

FIGURE 2.10: Testing the effect of the wavelength dependence of the Doppler shift. In green the residuals of two spectra, both rotational broadened once accounting for the wavelength dependence (slow) once without (fast). Over plotted in blue is the effect of a planetary transit. From left to right: 100 Å, 300 Åand 500 Å. As long as the wavelength section that is rotational broadened is below 100 Å, the influence on line profile is negligible.

The same code, as described in this section was used for observational data by replacing the synthetic data set with a real one which has been done for data on the HAT-P-2 (Section 4.2.1.1) and WASP-33 (Section 4.1.1) system.

2.2 Least Squares Deconvolution

Theory Least Squares Deconvolution (LSD) is a nice and stable way to solve an overdetermined system of equations numerically. In this chapter I will not go into much detail on notation and concepts of matrix computations. For the interested reader I recommend the following books: Matrix Computations [22], Numerical Recipes [23] and Inverse Problems in Astronomy [5].

Equations or functions that describe physical phenomena that have been observed with a spectrograph are in real world scenarios convolutions of different profiles. These profiles can be the spectrograph's instrumental profile, seeing caused by the moving atmosphere or the result of physical processes in the observed object. The observer therefore "sees" not the function $f(u)$ but the convolution of $f(u)$ with a broadening function:

$$h(x) = \int_{-\infty}^{+\infty} f(u)\, g(x-u)\, du \tag{2.7}$$

or when working with data usually a template is used that is then convolved with the assumed broadening to match the observation:

$$Template * Broadfunc = Observation. \tag{2.8}$$

So instead of "assuming" the broadening function, the basic principle of LSD is to deconvolve the spectra, by using a template to create a so called "design" matrix. The template can be a delta function template or sharp line template, containing preferably all the spectral lines that are observed at the correct wavelength position and with the depth representing their relative strength. It is also possible to use broadened templates to include other broadening mechanisms that are not desired to show up in the final deconvolution. This way only the rotational broadening can be reconstructed.

The design matrix itself is constructed by shifting the template vertically by one element for each row element. The number of row elements and shifts has to be predetermined. It should not be less than the number of bins a single line spans inside the spectra and at the same time not have too many elements. A rough estimate is the width of a single line plus 20 % extra bins. The number of elements has to be uneven. The resulting system of equations has then the form of an over-determined set of linear equations.

The next step is to use Singular Value Decomposition (SVD). The basic principle of SVD is that a matrix can be written as the product of three matrices. A given rectangular matrix $\hat{A}$ can be decomposed as:

$$\hat{A} = \hat{U}\hat{W}\hat{V}^T \tag{2.9}$$

where $\hat{U}$ and $\hat{V}$ are unitary matrices and $\hat{W}$ has the same size as $\hat{A}$ containing non-negative real entries. In principle $\hat{W}$ is a vector containing the diagonal elements.

Starting from:

$$\hat{Des}\,\hat{B} = \hat{P} \tag{2.10}$$

with $\hat{Des} = \hat{A}$:

$$\vec{B} = \hat{V}\,\hat{W}^{-1}\,\hat{U}^T\,\hat{P} \tag{2.11}$$

a deconvolution of the spectral broadening $\vec{B}$ function is achieved.

To quote Rucinski 1999 [53] there are advantages and disadvantages using the SVD approach:

> “On the positive side:
> (1) The problem can be treated as a set of linear equations.
> (2) An “inverse” of the rectangular array $\hat{Des}$ is possible.
> (3) The solution of $\vec{B}$ is defined in the least-square sense (shortest modulus).
> (4) The result is the real broadening function.
> But there are also minuses:
> (5) One must solve a large system of, say, 2000 equations of 200 unknowns.
> (6) One must know a priori how many unknowns.
> (7) Initially, the results may turn out quite poorly, because of the presence of plenty of linearly-dependent equations in the system (parts of the spectra where the featureless continuum provides no broadening information).”

For point (7) exists a neat solution. Small values in the diagonal matrix $\hat{W}$ are not desired and can therefore be removed. This results in the removal of the linearly dependent equations, removes the effect of noise, and reduce the number of unknowns. To test the effects of this and the ability of LSD to recover the broadening function for my intended usage scenario, the reconstruction of the planetary transit signal, see paragraph “Testing LSD”.

One way to visualize the results obtained with LSD is to plot the residuals of the resulting broadening functions and the mean broadening function as a color map with the x-axis representing the stellar rotation velocity, y-axis as the time axis and the color representing the z-axis (the deformation).

The Planetary Model Using a Keplerian model for the orbit a planetary track can be plotted onto the residuals color map and adjusted by hand to fit the planetary “bump”. Since the eye can easily be misled different combinations of orbital parameters can lead to an apparently good agreement. To counter this a fit routine based on the assumption that the planetary “dent” is a Gaussian was developed. Assuming that the literature values for the period, the semi mayor axis etc. are correct the code has four free parameters: the orbital inclination angle i, the misalignment angle λ, the amplitude of the Gaussian and the width of the Gaussian. The phase information of the individual spectra is used to decide if there is a “dent” which means the planet is in front of the star in regard to the observer, and where it is located on the stellar surface in terms of RV. The Gaussian is also scaled by a limb darkening coefficient according to the linear limb darkening law.

In principle it is also possible to set all parameters that define the Keplerian orbit around the host star as free fit parameters. Since the transit is only a short phase of the orbit, it is questionable if an extended fit will be stable. Also as already mentioned in Section 2.1 the planetary signal will be weak during the ingress and egress phase of the transit. If the code had the liberty to adjust other orbital parameters this could result in a shortened transit which then will be in conflict with the transit duration derived from light curve analysis.

Testing LSD Because a sharp line template was used, the broadening function calculated with LSD accounts for all the physical mechanisms that broadened the line profile. Also it includes some level of noise. As mentioned in the theory paragraph of this section, the width of the array given to LSD should not exceed the width of a single line in the profile to a large extend. If a too large number of bins is used the reconstruction gets almost perfect, but at the same time the resulting broadening function gets deformed. If a too small number of bins is used only the central region of the broadening is reconstructed and it also shows deformations. This is due to the fact

that the ”sampling“ of the profile gets more coarse. To reduce the effect of noise on the broadening function it is possible to discard singular values (SV) in the diagonal matrix $\hat{W}$. Rucinski 1999 [53] uses the factor of max(SV value) / min(SV value) as an estimation on how many SV can be discarded. Using this as a rule of thumb proved not feasible in my usage scenario. It is impossible to estimate the number of SV that can be discarded a priori. It has to be tested hands on if the noise in the broadening function gets reduced and how many values can be discarded.
To test the ability of LSD the same two simulations of the WASP-33 and the HAT-P-2 system described in Section 2.1 paragraph ”Testing the model” were used. For both simulations a Monte Carlo Markov Chain (MCMC) based fit was set up, calculating 50,000 steps each (Fig. 2.11,Fig. 2.12,Fig. 2.13,Fig. 2.14).

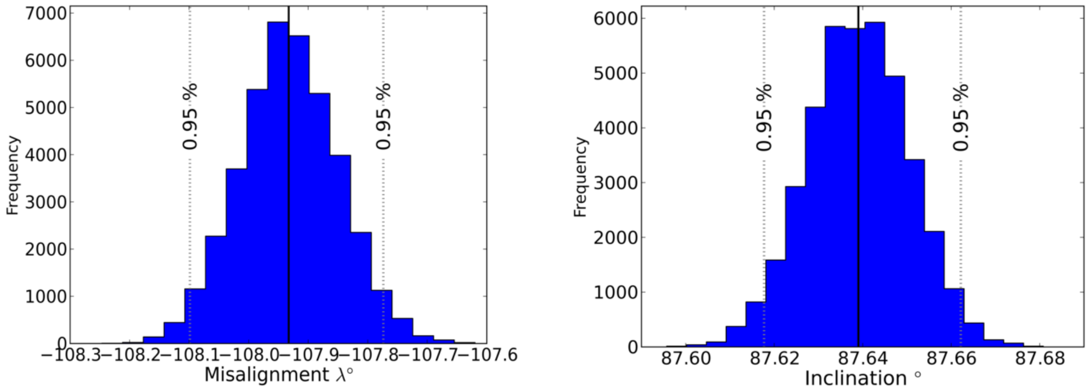

FIGURE 2.11: Frequency histograms for the inclination i and the misalignment λ of the MCMC calculation done for the WASP-33 transit simulation.

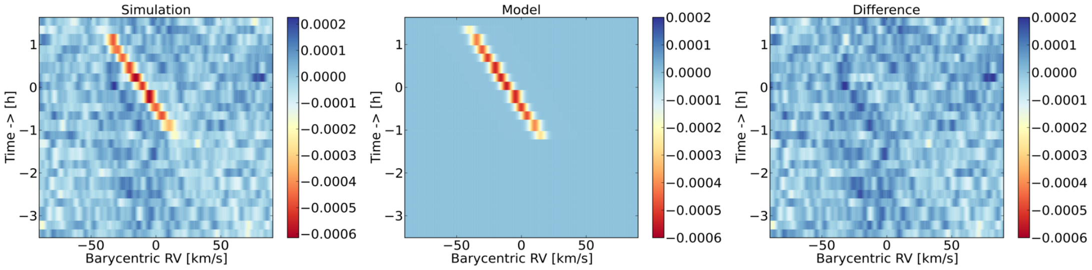

(a) The reconstruction of the deformation caused by the planetary transit.

(b) The best fit model to the data.

(c) The resulting map after subtraction of the model.

FIGURE 2.12: Residuals with respect to the mean LSD line profile of the WASP-33 simulation.

For the HAT-P-2 simulation, it was also tested if it is possible to recover the eccentricity and the argument of periastron passage ω which are linearly correlated. It proved to be impossible to recover the correct values for the eccentricity and the argument of

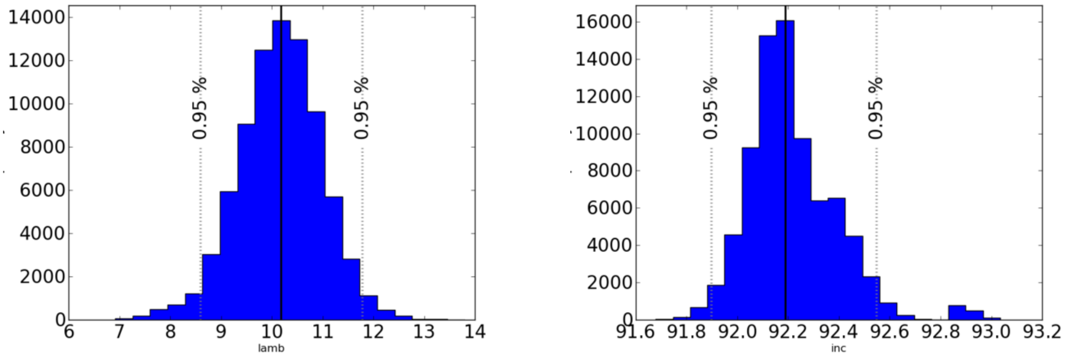

FIGURE 2.13: Frequency histograms for the inclination i and the misalignment λ of the MCMC calculation done for the HAT-P-2 transit simulation.

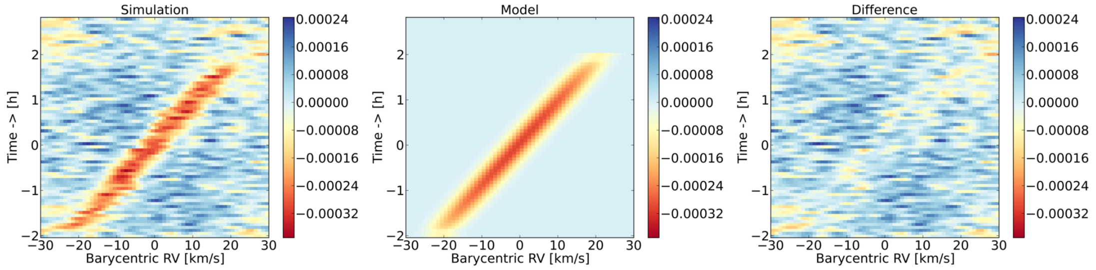

(a) The reconstruction of the deformation caused by the planetary transit.

(b) The best fit model to the data.

(c) The resulting map after subtraction of the model.

FIGURE 2.14: Residuals with respect to the mean LSD line profile of the HAT-P-2 simulation.

periastron passage ω. A explanation is that only a small part of the orbit is in transit, and therefore not enough data points are provided. It is advisable to use values determined by complementary methods that use the complete orbital solution of the system not only the transit phase.

When working with observational data, a correction for the motion of the stars on the sky and the motion of the Earth around the Sun has to be applied. The planet itself does perturb the system and this can have an effect on the spectra, if the transit occurs in a phase of the Keplerian orbit that has a large gradient in the velocity.

All this introduces a RV shift to the spectra. Several of these corrections can be calculated but also the wavelength calibration might introduce some offset value. During the stellar template creation this shift value has to be supplied to the code.

Due to the large value of vsini, WASP-33 is prone to have an error in the determination of the RV offset of the spectra. The line profile is broad and therefore a small change in RV does not degrade the goodness of the template fit. To this end I tested the influence of a change in this value on the fitted orbital parameters. I introduced an offset of one to five km/s in the case of HAT-P-2 and of two to 12 km/s in the case

of WASP-33. For each case a 50,000 steps MCMC fit was done. The final resulting orbital parameters for the inclination i and the misalignment angle λ were then plotted against the offset and fitted linearly. The resulting gradient gives an estimation on how large the effect is. For WASP-33 the effect on the misalignment angle λ is negligible and below the one σ error of the input values and for the inclination the value is 0.15 per km/s. For HAT-P-2 this results in a value of 0.40 per km/s for the orbit inclination i and 3.34 per km/s for the misalignment angle λ. The correct determination of the misalignment from observational data is hence strongly dependent on supplying the correct RV shift of the spectra in the case of the HAT-P-2 system.
Using LSD it was possible to recover the input values within the error margins, for both simulated transits (Table 2.1). The method is therefore more stable than the direct profile modeling approach even though it has more degrees of freedom. Less parameters are preferable since this leads to smaller statistical errors.

Table 2.1: Results testing the direct profile modeling (DPM) and LSD using a simulation with real system parameters. Each fit was done using a MCMC fitter using 50,000 steps. For WASP-33 LSD is able to recover the input values within the error bars. For DPM there is a slight offset to the input parameters. The λ DPM value for HAT-P-2 are completely inconsistent with the input values. The LSD result is again in agreement with the input values within the errors.

	HAT-P-2			**WASP-33**		
Parameter (Unit)	Input	DPM	LSD	Input	DPM	LSD
Orbital inclination, i (deg)	92	$95.6177^{+0.0151}_{-0.0251}$	$92.2156^{+0.3315}_{-0.3197}$	87.7	$87.4158^{+0.0064}_{-0.0065}$	$87.639^{+0.0232}_{-0.0213}$
Misalignment, λ (deg)	10	$90.95686^{+0.2741}_{-0.2692}$	$10.163^{+1.6143}_{-1.5702}$	-107.7	$-106.168^{+0.046}_{-0.048}$	$-107.932^{+0.158}_{-0.167}$
Limb darkening factor	0.71	-/-	-/-	0.6	-/-	-/-
Stellar rotation velocity (km/s)	21.3	-/-	-/-	87	-/-	-/-
R_{planet}/R_{star}	0.06891	-/-	-/-	0.1066	-/-	-/-
Semimajor Axis $/R_{star}$	10.28	-/-	-/-	3.79	-/-	-/-
Eccentricity	0.5163	-/-	-/-	0.0	-/-	-/-
Orbital Period (d)	5.63341	-/-	-/-	1.21986983	-/-	-/-
Argument of Periastron passage ω (deg)	189.92	-/-	-/-	90.0	-/-	-/-
Time of Periastron (JD)	2454213.4794	-/-	-/-	2454590.180251	-/-	-/-

Chapter 3

Observations

3.1 Telescopes / Instruments

This chapter gives a brief introduction on the telescopes and instruments used for the data acquisition. For more details I refer the interested reader to the included links to the respective web pages. The selection criterion was the availability of suitable data (either public or our own) or the possibility to propose observations for the instrument.

Calar Alto / CAFE Located in the Sierra de Los Filabres in Andalucia Spain, Calar Alto [7] has three telescopes with aperture sizes of 1.23 m, 2.2 m and 3.5 m. Calar Alto Fiber-fed Echelle (CAFE [6]) is a high-resolution echelle spectrograph fed through a fiber mounted at the Cassegrain focus of the 2.2 m telescope. The spectral resolution can be as high as 70,000 and the wavelength coverage is in the range from 3960 to 9500 Å. For the wavelength calibration a Thorium Argon or halogen lamb can be used.

Cerro Paranal / UVES The European Southern Observatory (ESO [16]) is located in the Atacama Desert in Chile with three sites: La Silla, Paranal and Chajnantor. Located at Paranal is the Very Large Telescope (VLT) consisting of four 8.2 meter class telescopes and four 1.8 m Auxiliary Telescopes. Mounted at the UT2 is the Ultraviolet and Visual Echelle Spectrograph (UVES [17]). UVES has a spectral resolution ranging from 40,000 to 80,000/110,000 (blue/red). The wavelength coverage is 3000 to 5000 Å in the ultraviolet and 4200 to 11,000 Å in the visual. For wavelength calibration a Thorium Argon lamb or a Iodine Cell can be used.

Keck / HIRES There are two telescopes, Keck I and II which both have a main mirror diameter of 10 meter and are located at the top of the Manua Kea in Hawaii and part of the Manua-Kea-Observatory. The High Resolution Echelle Spectrometer (HIRES [29]) is mounted at a naysmth platform with a possible resolution between

25,000 to 85,000. The wavelength calibration is done with an iodine cell. HIRES spectra, if available, might only be partly usable for LSD or the direct analytic approach, without proper removal of the iodine lines, or only using the CCDs without any iodine lines (CCD one and three, HIRES has three CCDs in total). An iodine cell also results in a reduced S/N ratio of the spectra.

Observatoire de Haute - Provence / SOPHIE The Observatoire de Haute - Provence [42] is located in the Alpes de Haute-Provence in the southeast of France at an altitude of 650 meters. There are several telescopes on site including aperture sizes of 1.93 m, 1.53 m, 1.20 m and 0.8 m. The cross-dispersed echelle spectrograph [43] is fiber fed with light coming from the Cassegrain (f/15) foci of the 1.93 m telescope. The spectrograph has two modes of operation: a high resolution mode (HR) with a spectral resolution of 75,000 and a high throughput mode (HE) with a spectral resolution of 40,000 which can be used for faint targets. A wavelength range of 3872 to 6943 Å can be covered. For wavelength calibration a Thorium Argon or tungsten lamb can be used mounted at the Cassegrain.

HATNet / SuperWASP Both are dedicated missions to detect transiting exotrasolar planets, including the planets of which I analyzed follow-up high-resolution observations. The Hungarian Automated Telescope Network (HATNet [24]) uses a network of six small (11 cm diameter), wide-field (8x8 deg) telescopes and has been operational since May 2001. In 2009 HAT-South was added each consisting of eight astrographs (18 cm diameter) with overlapping field of view. So far 29 exosolar planets have been discovered using HATNet. SuperWASP (Wide Angle Search For Planets [59]) has two sites each using a setup consisting of eight small telescopes (20 cm diameter) and has a sky coverage of 500 square degree. More than 80 planets have been discovered so far.

3.2 Target Selection

In this section a list of all currently known planetary target candidates for using the methods described in Chapter 2 is presented. Here, I give the applied constrains, if data are available in the various archives or the possibility for proposing additional observations exists.

Constraints The same constraints as for Doppler Imaging apply. A sky projected stellar rotation velocity (vsini) of $\approx$ 20 km/s or higher is needed, a high spectral resolution $>$ 50,000, a signal to noise ratio ration (S/N) of $>$ 100, a large planet,

Table 3.1: Planetary candidates for LSD / Direct fitting approach. Stellar rotation velocity (vsini) values are rounded. Observed stands for that high resolution spectra exist and which spectrograph was used for the observation. For KOI-13 the Kepler magnitude is listed. The star behind the checkmark for WASP-7 and XO-3 means that only prelimilary results will be presented in the Chapter 5.

Planet	Vsini (km/s)	V mag	Rp/Rs	Orbit Period (days)	Observed?	Analyzed
COROT-11b	40	12.8	0.107	2.994	HIRES	X
HAT-P-2b	21.3	8.7	0.0722	5.633	HIRES	✓
					SOPHIE	✓
HAT-P-34b	24	10.2	0.0801	5.452	HIRES	X
HAT-P-41b	19.6	11.4	0.1028	2.694		
KELT-1b	55	10.7	0.078	1.2175		
KOI-13.01	40	> 9.958	0.0908	1.763		
WASP-7b	17	9.5	0.0760	4.954	UVES	✓*
WASP-33b	87	8.3	0.1065	1.219	CAFE	✓
WASP-79b	19.1	10	0.1071	3.662		
XO-3b	18.3	9.9	0.0945	3.191	HIRES	✓*
					SOPHIE	X
					HDS	X

and an exposure time of around 600 seconds or shorter, to counter phase smearing. The required high value for vsini reduces the target list significantly. If the target's host star is too faint, a good signal to noise cannot be achieved within a reasonable observing time. For instance almost all Kepler detections have host stars that have magnitudes fainter than visual magnitude (V mag) 10, typically between 14 and 15 Kepler magnitudes. Kepler magnitude values are comparable to visual magnitude values. There are two telescope sites equipped with a high resolution spectrograph and where an application for observing time is possible for me. One is the ESO site at Cerro Paranal and the other site is Calar Alto (Section 3.1). For Calar Alto no stars fainter than $V = 10$ deliver the required S/N and for an eight meter class telescope like the VLT the magnitude should not be fainter than a $V = 12$.

Candidates My research resulted in a candidate list of ten planets (Table 3.1). For four planets there is publicly available data: COROT-11b, HAT-P-2b, HAT-P-34b, and XO-3b. For WASP-7b and WASP-33b I had access to our own data.

In the case of COROT-11b Gandolfi et. al. 2011 [18] have already applied Collier Cameron's "Line Profile Tomographie" method to the available data, so no further work was done in the course of this thesis.

For the HATNet discovered planet HAT-P-2b there are high resolution spectra available from two different spectrographs SOPHIE and HIRES. I analyzed the SOPHIE HAT-P-2 data set (Section 4.2.1) and furthermore the HIRES data set (Section 4.2.2) to assess the possibility to use data sets including iodine cell contamination.

Possible Cerro Paranal targets include HAT-P-34b, HAT-P-41b, WASP-7b and WASP-79b. High resolution spectra of HAT-P-34b are available (Bakos et al. 2012 [2]). However, the mid transit phase is missing from the data set. Also HAT-P-41b fits the required high vsini, with an apparent magnitude of 11.087 it is close to the S/N limit. As HAT-P-34b, this possible target was discarded in preference for WASP-7.

Since the Super-WASP discovered system WASP-7b offers not only the possibility to use the direct profile modeling approach and LSD, but also to measure differential rotation. The scientific case for observations is much stronger and we decided to propose for WASP-7. The WASP-7 system is an interesting case with a misalignment angle λ of nearly 90° ($\lambda = 86°$). Also the orbital inclination i is 87.7°. This results in a transit that does not cross the rotation axis of the star. The system is excellent to measure differential rotation and the stellar limb darkening. Since the planet crosses the star almost in parallel to its rotation axis, the surface velocity at each latitude is mapped by the transiting planet. Differential rotation would result then in a nonlinear RV shift of the planetary signal. I used my transit code to simulate a transit including differential rotation. Using LSD to recover the broadening function the planetary signal showed the presence of differential rotation by being “banana” shaped as expected (“Differential rotation of WASP-7” (ESO VLT/ UVES 91CfP) Appendix B). The differential rotation part is not part of this thesis. However I present some preliminary results of the application of LSD in Section 5.3 of this thesis.

An interesting target for future work on this topic might be WASP-79, a Cerro Paranal Winter object.

Possible Calar Alto targets include KELT-1 and KOI-13. Even though their respective stellar rotation velocity is high they might be too faint to achieve the required S/N. For WASP-33b, another Calar Alto target, I had access to high resolution spectra obtained using CAFE (Section 3.1) and the results are presented in Section 4.1.

In the case of XO-3 there is data available from three different spectrographs and I did some preliminary work on the available HIRES data (Section 5.3).

3.3 Data Reduction

This chapter describes the methods used for the reduction of the data (if not already available), how the normalization was done and the steps for obtaining a stellar template needed for the direct profile modeling approach (Section 2.1) and for Least Squares Deconvolution (Section 2.2).

> **Correct time(s)?** There is one important aspect to always be careful with: the correct declaration of time. The standard in astronomy is to list times as Julian dates (JD) but there are several time standards for JDs and they are easily confused. I will not go into too much detail and only mention the most commonly used standards. I refer the interested reader to Eastman et al. 2010 [15] for a detailed description of the different time standards. There are also handy online applets provided by Eastman [14] for time standard conversion.
>
> If only JDs are listed they are most probably in Coordinated Universal Time (UTC). HJD stands for Heliocentric corrected JDs and BJD stands for Barycentric corrected JDs and they are location dependent both. For data needing highest precision, like pulsar timing, BJD is used. The difference between HJD and BJD is up to 8 seconds. Also with HJD the result depends on the algorithm used. Both can be either in UTC or in Barycentric Dynamical Time (TDB) which are the two most commonly used time standards. The difference between UTC and TDB is 32.184 + N seconds. The N stands for the number of leap seconds and has to be adjusted accordingly to the observation date.
>
> In 1991 the International Astronomical Union (IAU) decided in the resolution A4 to favor BJD over HJD.

3.3.1 Reduce

REDUCE is a data reduction software package written in IDL by N. Piskunov and J. Valenti [48] mainly aimed at the UVES spectrograph, but it can also be used for other instruments. There are several steps in the reduction process using REDUCE which cover the BIAS (background noise due to currents in the readout equipment), FLAT fields (to balance the relative response of each individual pixel and remove artifacts caused by the optics), DARK currents (thermal noise of the CCDs), order tracking, wavelength calibration (iodine cell / lambs) and BLAZE calibration (needed due to the different intensities in each order caused by the geometry of the echelle grating).

As a first step the orders on each raw image are defined. REDUCE fits high order polynomials along each order and constructs an order definition file which is used to build a normalized flat field. The same is done with the Thorium Argon spectra. The next step is to do the wavelength calibration using the Thorium Argon spectrum and match it with a template spectra of Thorium Argon through the help of a GUI based tool called WAVECAL. This is done order by order. In the next step the 1D spectra are extracted based on the order definition file and the BLAZE correction is applied. The final step is to add the calibrated wavelength solution to the spectra using WAVECAL.

3.3.2 Normalization

Instead of relying on an automatic normalization a manual normalization of the spectra was done.

As a first step the mean of all phases was divided by a stellar template based on a normalized Kurucz model atmosphere [32]. This is based on the assumption that if the difference between a normalized template and the observed spectrum is a factor A, then by dividing the observed spectra by a given template, A is one in the case of perfectly fitting template. Since the observed spectrum is not yet normalized, A will differ from one. The knowledge of A can then be used to normalize the observed spectra by dividing the spectra through the factor A. In reality this only works for the continuum since the template is never going to fit perfectly. Over plotting the mean spectrum with the Kurucz template helps to find these points of continuum. Each phase was then divided by its own sum and by the spline fit through the assumed points of continuum. Finally the resulting spectra were divided by their mean, respectively. Using this method a, in regard to the mean of all phases, stable normalization over time can be achieved.

To be able to do the normalization by hand, I developed a Python matplotlib based GUI tool (Fig. 3.1). Variations of the tool were used for the different data sets. Points can be added or removed and the code will apply a cubic spline fit through these selected data points (Fig. 3.1(a)). The result can be saved inside a Python dictionary and be reloaded for later use or comparison. In a second plot window the resulting normalization is shown (Fig. 3.1(b)). With a slider the spectra can be selected and the plot will change accordingly. Through this GUI tool the goodness of the normalization can be checked over time and verified.

In a separate program the mean of the resulting normalization spectra is fitted by using a multi-Gaussian fit (Section 3.3.4) based on a line list calculated using SPECTRUM [20]. In the GUI tool also a fit result display mode has been included which makes it possible to check on the result of the multi-Gaussian fit in comparison with each phase and the mean of all phases (Fig. 3.1(c)).

3.3.3 Outlier Removal

In order to do the normalization any outliers present in the data have to be removed. Either these outliers can be hot pixels or they are artifacts of the data reduction process. There is an automatic outlier removal code included in PyAstronomy [11]. It first computes the “distances” between adjacent bins and then uses an algorithm based on the Generalized Extreme Studentized Deviate (ESD) test for identifying outliers in

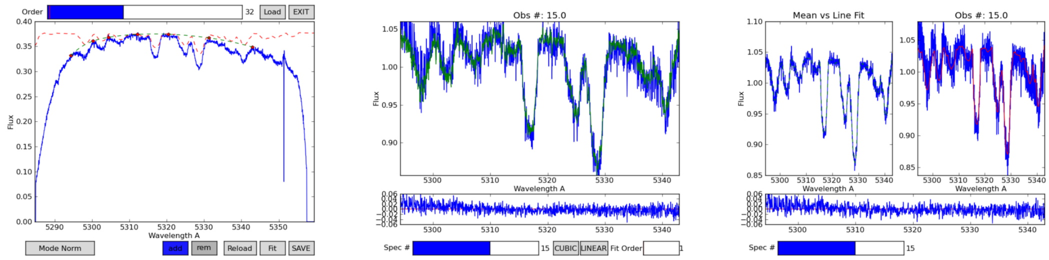

(a) Main window of the GUI tool. (b) Secondary window of the GUI tool normalization mode. (c) Secondary window of the GUI tool fit mode.

FIGURE 3.1: Matplotlib based interactive GUI tool for the normalization. The version used for the WASP-33 data is shown.

a univariate normally distributed data set to find the distances that are abnormal (Rosner 1983 [51]). Since the code did not detect all outliers because some show low gradients I also removed some outliers by hand using a GUI based matplotlib tool I programed for this purpose (Fig. 3.2).

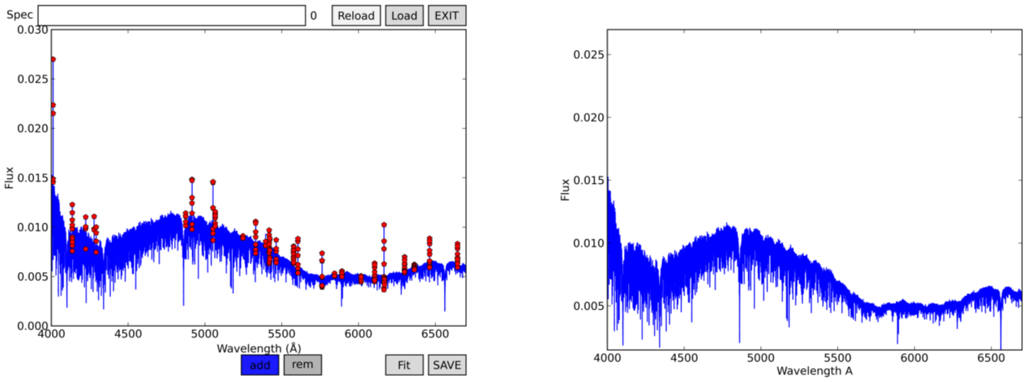

(a) Main window of the GUI tool. Points can be added / removed by hand (b) Secondary window of the GUI tool showing the result of the outlier removal

FIGURE 3.2: Matplotlib based interactive GUI tool for outlier removal; As an example the HAT-P-2 SOPHIE data is shown.

3.3.4 Stellar Template

In order for the direct profile modeling (DPM) approach and LSD to work, a stellar template is required. In case of the DPM an non-broadened profile is needed. First tests were done with a scaled PHOENIX [25] template. Since the PHOENIX template is rigid and no individual lines can be adjusted, only small regions could be fitted. This approach is also not applicable for LSD for our particular usage scenario of fast rotators. For fast rotators the broadening is dominated by rotation, other broadening mechanisms do not have a significant influence on the profile, therefore there is the need for a sharp line profile.

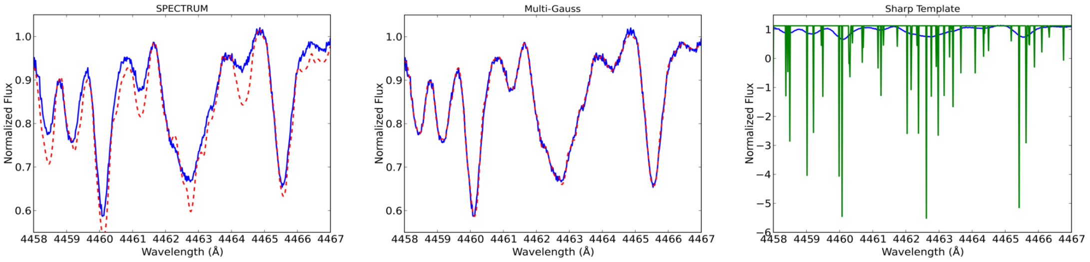

(a) SPECTRUM synthesized result for the HAT-P-2 system parameters. In blue the mean of all phases, and in red the result from SPECTRUM.

(b) Multi-Gaussian fit result for the HAT-P-2 dataset. In blue the mean of all phases, and in red the best fit.

(c) Sharp line template obtained from the multi-Gaussian fit. In blue the mean of all phases, and in green the template.

FIGURE 3.3: Steps to obtain multi-Gaussian based templates.

I used the following three steps to get a template:

A. To get a first estimation on the strength of each absorption line, SPECTRUM [20] was used to calculate a stellar template considering the physical properties of the host star, e.g. temperature, log_g etc. (Fig. 3.3(a)). Based on this template a line list was created including the position, the strength and the equivalent width of each line.

B. In a next step the amplitude of each absorption line was adjusted using a multi-Gaussian fit to improve the fit to the mean spectrum of each data set. This can be done since the physical effects that caused the line depth and shape are irrelevant for my methods and for fast rotators, the profile of the lines is dominated by the rotational broadening. It is only important that the template fits well to the spectra and the position of the lines is correct in the wavelength domain (Fig. 3.3(b)).

C1. For the DPM approach the non broadened Gaussian is saved as a stellar template, preferably in higher resolution then the observation.

C2. For my usage scenario of LSD a sharp line (delta function) template is needed that gives an estimation of the line positions and line strengths. Using the line position information of the line list a template is created that is based on the bin size and wavelength range of the observation. For each line list entry the amplitude is written into the closest bin and normalized by dividing through the size of the bin so the equivalent width is correctly reproduced (Fig. 3.3(c)).

In case of a slow rotator other broadening mechanisms such as temperature, pressure, van-der-vaals broadening etc. influence the line profile. Using a Gaussian is then no longer sufficient to get a good fit, because the code has problems fitting the wings of the lines. To improve the goodness of the fit a multi-Voigt profile fit can be used in this particular case.

Optimized Template Since the sharp line template is never perfect, the reconstruction of the line profile shows some deviations from the observed spectra. The following approach was tested to optimize the template:

A. The mean of all phases was taken as observation.

B. LSD was used to get a reconstructed profile.

C. The depth of the sharp line template was adjusted to improve the reconstruction.

This improved the reconstruction at the position of strong lines to some small extend. There is no clear indication for an improvement in the final solution and furthermore the optimization takes a lot of computation time (each time a LSD profile has to be computed). To conclude no further optimization was done for the template creation.

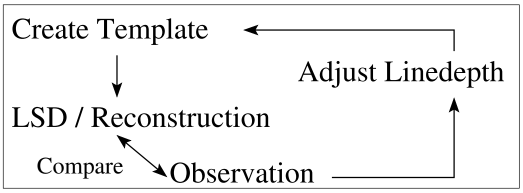

SME As a second approach for slow rotators it was tested if Spectroscopy Made Easy (SME) can be used to obtain an improved template, instead of using a multi-Voigt profile fit. SME is an interactive fitting tool written in IDL by Valenti and Piskunov [62] that synthesis spectra using a VALD line list [61]. Different physical parameters can be fitted such as the stellar temperature, logg etc. . In the recent years it has become quite popular to use SME for the determination of the physical properties of an observed star. It is possible to extract the best fit result as a improved VALD line list, which makes SME interesting in my case.

The first step that has to be done is to fit the oscillator strength of strong lines to a solar template. The values given by VALD are for laboratory measurements and have to be adjusted. Following this step this new line list can then be fitted to the observed spectra of the to be analyzed star with the oscillator strength derived in the previous step.

In comparison to the results obtained using a multi-Gauss or multi-Voigt profile, the line profile obtained using SME is differing from the observed spectra not only in the line depth but also has problems representing the wings correctly. Another problem is that the fitting is time consuming even when only small wavelength regions are fitted at once. This is caused by the fact that SME synthesizes the spectrum for each fit in the complete wavelength range. Using then the resulting line list from SME produced deformed mean line profiles in the case of LSD. It was therefore decided that the multi-Gauss and multi-Voigt fit approach is preferable. The idea to use SME did not give a satisfying result.

Chapter 4

Results

4.1 WASP-33

The System The planet WASP-33b orbits a fast rotating A5 Delta Scuti star (HD15082, $Vmag = 8.3$, $vsini = 87.22\ kms^{-1}$) in a 1.22 day orbit. It is to date the only planet hosting star that shows pulsations. The planet/star size ratio is 0.1066 and due to the close in orbit it is highly inflated. It was discovered using SuperWasp in 2006 (Christian et al. [8]) and confirmed spectroscopically by Collier-Cameron et al. in 2010 [10], who did also some photometric follow up observations.

The high rotation velocity and the large planet make it a good target. A large rotation velocity of the host star results in a better time resolution of the planetary signal due to the broad line profile (the planetary signal moves through several bins on the spectrograph) and a larger planet results in larger "bump" due to the planetary transit.

Due to the fast rotation of the host star, a confirmation using the RV method is not possible. Any shift of the line centers will be blended in the broadness of the line profile. This also effects the possibility of using the method of Ohta et al.2005 [44] or Hirano et al. 2010 [26] to extract the systems misalignment angle λ. As pointed out by Collier-Cameron et al. and Smith et al. 2011 [58] the pulsations additionally make accurate RV and photometric measurements challenging. Only a lower limit for $M\ sin(i)\ < 4.59 M_{Jup}$ is known and therefore the eccentricity of the system is unknown. In their paper Smith et al. favor a value of zero for the eccentricity due to the large radii of the planet and star and their close in orbit. They calculate a time scale for the circularization of $\tau = 1.72\ Myr$ which is well below the age of the system of about 500 Myr.

Instead of using the RV methods Collier-Cameron et al. proposed a technique they coined as Line Profile Tomography for hot fast-rotating host stars. By the means of

LSD they reconstructed a mean line profile in which a “bump” caused by the transiting planet is visible (Fig. 4.1).

> **Delta Scuti** stars are main sequence stars that are located inside an “instability strip”, the starting point of burning He. They show pulsations radially and non-radially. Radial pulsations result in a brightening and dimming of the star over time, due to the fact that the star increases in size and then decreases again. In the non-radial case, parts of the star move inward, while simultaneously parts move outward. The pulsations are in the milli-magnitude range and the frequency in the range of an hour.

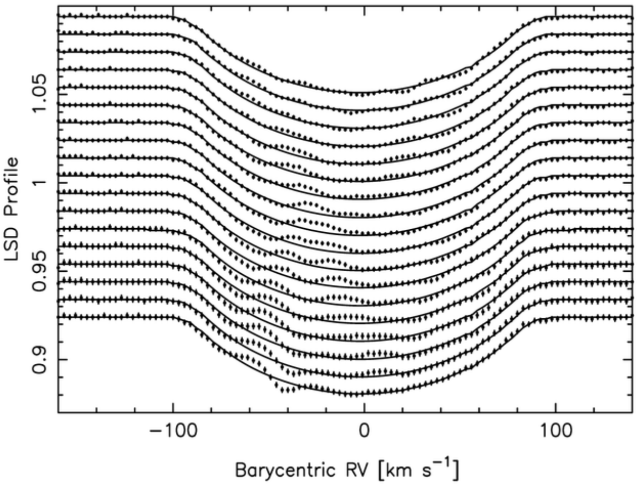

Figure 4.1: Mean profile reconstruction of WASP-33b planetary transit by Collier-Cameron et al. 2010 [10] using LSD. The transit was observed 2009 December 08 at the NOT. Overplotted as a solid line is the limb-darkened stellar rotation profile. The y-axis is the time axis. The planetary bump is clearly visible starting at the lowest profile at $\approx 5km/s$ and going up to $\approx 40km/s$ in the topmost profile.

The Data The following analysis is based on observations collected at the Centro Astronomico Hispano Aleman (CAHA) at Calar Alto, operated jointly by the Max-Planck Institut für Astronomie and the Instituto de Astrofisica de Andalucia (CSIC), during the night of 5th to 6th December 2011 using the CAFE spectrograph (Section 3.1) mounted at the on site 2.2m telescope. The observing time has been granted as part of the CAFE GTO time of the Institute for Astrophysics, Goettingen.

The data set shows a S/N ratio varying between 25 to 80, depending on the wavelength and the phase, therefore a relatively large planet results in that the low S/N is less of a problem.

The data reduction was done with the REDUCE software package (Section 3.3.1) by Carolina von Essen a member of our group. For wavelength calibration a Thorium Argon lamb was used with spectra taken prior to the science exposure. A number of

24 spectra were taken each with a duration of 600 seconds resulting in 12 during transit and 11 before and one after the transit based on the planetary rotational period from Smith et al. [10].

The Normalization The normalization proved challenging since WASP-33 has a high stellar rotation velocity vsini of about 87 km/s and even thought it is a class A star which results in less absorption lines, there is no visible continuum, only blended lines. Additionally the blaze correction done with REDUCE is not perfect since the orders are still deformed. This is not a problem of REDUCE itself but of the blaze function being not perfect, a result of the blended lines.

The first attempt to normalize small sections of the spectra by using a linear fit and then fit a PHOENIX spectra to the data resulted in only 167 Å of usable data, since it is only possible to scale sections of the PHOENIX template not individual lines. A linear fit as basis for the normalization also works only for small wavelength sections since it is not able to follow the curvature of the deformation of the order. Using only these sections as basis for testing the direct profile modeling approach did not give consistent results that point in the direction of the literature values. To get larger sections normalized a different approach was used, as explained in Section 3.3.2. A total of 2245 Å could be normalized with this method containing sections ranging from 20 to 40 Å per order.

The Template For the template a multi-Gaussian fit based on a line list was done to the normalized mean of all observed 24 phases (see Section 3.3.4). One could argue that it would be advised to use the off star spectra only since the planetary transit has an influence on the line shape. Since the star shows pulsations, these are also fitted and the idea behind using all 24 phases is that this negates some of the deformations caused by these pulsations, which are present in off and on star spectra both.

The width of the Gaussian was fixed to the values given by the line list. The amplitude and some scaling factors were the only free parameters. Using a Gaussian to create a template can be done since the rotation velocity of the host star is so large that individual lines are not important and what looks like a single line in the spectra is in reality a blend of multiple absorption lines. The width of these blends can be up to several Å. As the linear limb darkening parameter 0.6 and for the stellar rotation velocity 87 km/s was used.

4.1.1 Direct Profile Modeling

Due to the nature of the host star, the WASP-33 data have two main problems: one is the normalization (Section 4.1) and the other one is the pulsations of the host star, which is a Delta Scuti. The results obtained using Least Square Deconvolution (Fig. 4.3(a)) suggest that the deformations in the line profile caused by the pulsations are at least of the same magnitude as the planetary signal or might even be of higher magnitude. Since the direct profile modeling approach cannot distinguish between a deformation due to a planetary signal and a deformation that is the result of a pulsation, the fit finds more then one planetary track in the data.

Clearly there seems to be a local reduced χ^2 minimum close to the location of the literature values (Fig. 4.2(a)). Also there is a second region with a local minimum in the reduced χ^2. Comparing the orbital inclination i and the misalignment angle λ of this region with the results from LSD (Section 4.1.2) it becomes apparent that the direct fitting approach runs into one of the pulsations and, as a result, finds a second (pseudo) planetary signal. There is one strange phenomenon that also shows up in the reduced χ^2 maps. The fit seems to prefer that the planetary signal is absent, as the lowest reduced χ^2 values are in the parameter space where the planet is off star and the code returns an undeformed profile.

Reducing the planetary size solves this problem but not in a physically correct sense since the planet has to be reduced by about half its size, which is unreasonable and not within the error margins of literature values. It is unknown what causes the best reduced χ^2 values to occur in the parameter space where no planet is present. A simulation done with WASP-33 system parameters could not clarify the reasons for the part failure of the method (Section 2.1). As with real data there is a minimum around the input values but also the lowest reduced χ^2 values is in a region where the planetary transit signal is absent (Fig. 2.6).

To test if the minimum region around the literature values is not an artifact, the phase information of each spectrum was permuted in the sense that for the on star spectra the phases of the off star were used, and for the off star spectra the phases of the on star. Clearly the planetary signal disappears (Fig. 4.2(b)). Still, orbital parameters resulting in no transit show lower reduced χ^2 values. To remove any artifacts from the maps resulting from systematic effects introduced by the model both maps were subtracted. Two bumps remain: one around the literature value of the planetary signal and one at the position of one of the pulsations that is also present in the LSD maps (Fig. 4.2(c)). It is therefore appropriate to conclude that the assumption, that one minimum represents the planet, and one represents a pulsation is correct.

To get an estimation on the errors for the fitted parameters a 200,000 steps MCMC fit was carried out. The resulting parameters match the ones obtained with LSD, within the errors (Table 4.1). Since the method has fewer free parameters, the position of the planetary signal is statistically better defined, and therefore the errors are smaller then the ones obtained using the LSD planetary model.

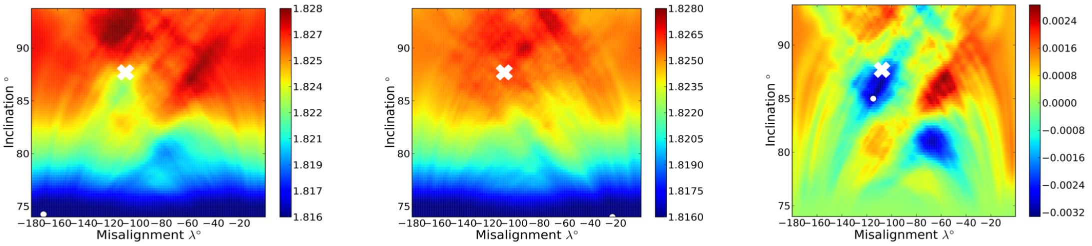

(a) The map shows a local minimum around the location of the literature values. Nevertheless the lowest reduced χ^2 value is found for an off star position.

(b) For this calculation the phase information was permuted in a way that off star phases are on star and off star are on star. Clearly the planetary signal vanishes.

(c) Resulting reduced χ^2 map when subtracting the previous two maps for the direct fitting approach. Clearly there are two distinct regions one around the literature values, the other for the position of one of the pulsations.

FIGURE 4.2: Reduced χ^2 map for the direct fitting approach applied to WASP-33. Only the inclination and the misalignment angle λ were varied for each phase. The white cross marks the literature values. The white circle marks the position of the lowest χ^2 value

4.1.2 Least Squares Deconvolution

The LSD approach was tested with two versions of the data: First, for each of the echelle orders the broadening function was reconstructed and the results added up. This has the advantage that the spectra do not have to be merged, which can cause problems in the overlapping regions due to differing normalizations and an imperfect wavelength calibration.

Second, since the normalization of the echelle orders of WASP-33 was found to be stable at the start and end of each order of each phase, the influence on the final result by merging the spectra into one over the whole normalized wavelength region was tested.

There is no change in the final result for the orbital parameters when a comparison between both approaches is done. The comparison shows that it is possible to do a LSD reconstruction for small wavelength regions and to add up the resulting reconstruction of each order, without resulting in a differing broadening function.

For both approaches the wavelength range was interpolated to a log-scale wavelength range where each $\Delta\lambda$ results in a velocity of 1 km/s. This was done since the Doppler shift is wavelength dependent.

One of the advantages of LSD is that by discarding singular values (SV) noise can be removed from the reconstruction. Both approaches show that with the WASP-33 data set it is impossible to remove any SV justified. Removing e.g. four values does not significantly reduce the noise, removing more than eight, the shape of the broaden function starts to show deterioration. The total number of SV was 201.

Based on the planetary model described in Section 2.2, a MCMC fit was done to the reconstruction using 500,000 steps. The residual map clearly shows the planetary transit signal going from top left to bottom right in a retrograde orbit (Fig. 4.3(a)). There are also several tracks visible that are caused by the pulsations. After subtracting the best-fit model (Fig. 4.3(b)), only the noise and the pulsation remain (Fig. 4.3(c)).

Since WASP-33 is a fast rotator, the reconstructed broadening function is dominated by the rotational broadening. Other broadening effects such as temperature broadening have negligible effect on the shape. It is possible to do a fit to the mean of all resulting broadening functions to extract the stellar rotation velocity. The best-fit value is 87.22 km/s. The level of error is hard to predict and remains unknown. The reconstructed profile includes some level of noise, including the noise of the spectra, and it does fix flaws in the template. The data also show the presence of the pulsations and the planetary transit signal. Nevertheless, when comparing the value with the literature value of Collier Cameron et. al., the result is compatible.

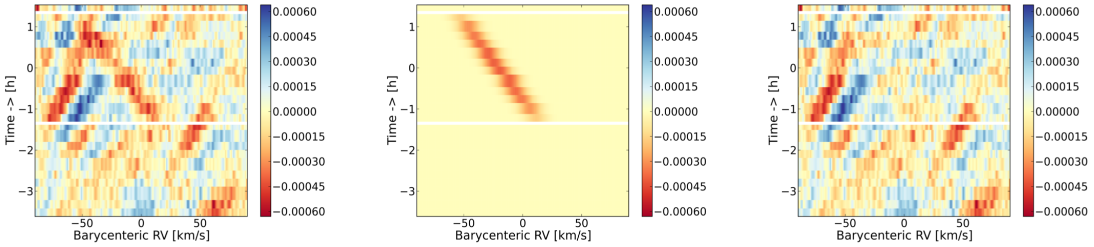

(a) The result for the observation

(b) The best fit planetary transit model using MCMC

(c) Subtracting the planetary transit model from the data

FIGURE 4.3: LSD residual maps calculated for the CAFE WASP-33 data set. The white lines mark the position of the begin and end of the transit according to Smith et al. 2011 [58]

4.1.3 Discussion

I used two independent methods to reconstruct the values of the orbital inclination i and the misalignment λ. Both methods result in parameters that are in agreement within their error boundaries.

In the case of DPM, a big question mark on the reliability of the methods remains. The reason for the preference of the fit that there is no transit in the data is unclear. Without the confirmation from LSD, the local minimum around the literature values could possibly be a pulsation and not a deformation due to a planetary transit. At the same time, the second local minimum could be mistaken for a planetary transit signal. The resulting map of the LSD reconstruction shows pronounced structures, which start at negative and go to positive RVs. These are caused by the pulsations of the host star (Fig. 4.3(a)). Only during the transit phase, there is a additional signal going in the opposite direction. With LSD the deformation of the line profile due to the planetary transit is clearly visible in the data. The planetary model in the case of LSD works reliably and proved to be stable. Due to the orbital configuration of the system, with the planet being in a retrograde orbit, there is a clear separation between what is a planetary signal and what is a pulsation. With DPM this visual inspection remains impossible. The user has to trust that the model fits the data correctly. Without a priori knowledge on the systems orbital parameters or in the case that the known values have large error bars it is not possible to use DPM standalone.

Comparing my results to those obtained by Collier-Cameron et al. and Smith et al. I find good agreement (see Table 4.1). The retrograde planetary bump is at a comparable position and there are pulsations of similar strength going the other direction (Fig. 4.3(a)). The result for the misalignment angle λ is off by one degree, in regard to the result by Collier-Cameron et al. but this is most probably the result of the differing inclination value. My model returns smaller errors for the inclination and larger errors for the misalignment. Also Collier-Cameron et al. used data from three different spectrographs to get their final result, whereas I had access to a single data set only. My result is an independent confirmation of the misalignment of the system using a different telescope and spectrograph.

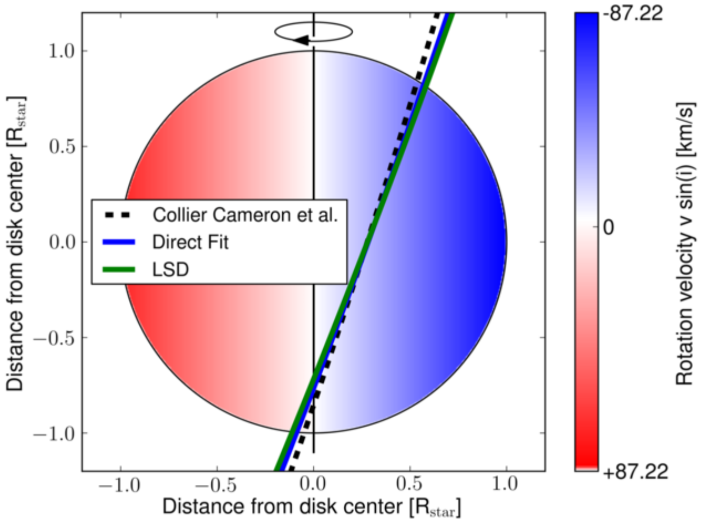

FIGURE 4.4: Visualization of the planetary track on the stellar surface of WASP-33 for the literature values by Collier-Cameron et al. 2010 [10] and the results form the direct profile modeling and the LSD reconstruction.

TABLE 4.1: WASP-33 system parameters. DPM stands for direct profile modeling approach and LSD for Least Squares Deconvolution. The star stands for the usage of the literature values by Smith et al.

Parameter (Unit)	Collier Cameron	Smith	This work	
			DPM	LSD
Orbital period (d)	1.2198669 ± 0.0000012	$1.21986983 \pm 0.00000045$	*	*
Epoch of mid-transit (HJD)	$2454163.22373 \pm 0.00026$	$2454590.17948 \pm 0.00028$	*	*
Orbital inclination, i (Degree)	87.67 ± 1.8	$84.9^{+2.1}_{-1.7}$	$86.078^{+0.042}_{-0.050}$	$86.0497^{+0.1552}_{-0.1634}$
Misalignment, λ (Degree)	-107.67 ± 0.57	-/-	$-109.401^{+0.218}_{-0.251}$	$-110.962^{+1.013}_{-1.058}$
Stellar radius ($R_\odot$)	1.444 ± 0.034	$1.512^{+0.060}_{-0.054}$	*	*
Planet Radius (R_{Jup})	1.497 ± 0.045	$1.501^{+0.073}_{-0.064}$	*	*
Transit depth (R_{planet}/R_{star}	0.01066 ± 0.0009	$0.01041^{+0.00023}_{-0.00021}$	*	*
Orbital major semi-axis, a (AU)	0.02555 ± 0.00017	0.02565 ± 0.00023	*	*
Stellar rotation, vsini (km/s)	86.05 ± 0.06	-/-	87.22	87.22

4.2 HAT-P-2

The System HAT-P-2 (HD147506) is the second transiting exosolar planet discovered by the HAT-Net with an orbital period of 5.644 days. When discovered in 2007 (Bakos et al. [2]), it was the most massive, longest period and eccentric exosolar planet known. The host star has a spectral type of F8 with a visual magnitude of 8.7 and a stellar rotation rate of about 21.3 km/s. Both make the system a good target for my methods to reach the required S/N and also to have a rotational broadening dominated spectrum.

At the orbital distance of the system the transit probability is about 10 % for such a massive object. As of today, there are 42 systems known with planetary masses above 9 M_{jup} and 51 systems, with eccentricities of 0.5 and larger (Fig. 4.5). As pointed out by Loiellet et al. (2008 [35]), the high density (11.9 gcm^{-3}) and surface density (227 ms^{-2}) could result in an object that is close to being a brown dwarf.

The high eccentricity of the system makes it an intriguing target, since this is usually observed for giant planets in large orbital distances not for close in planets like HAT-P-2b. Lewis et al. (2013 [33]) find hints for the presence of another sub-stellar object in the system that could have caused the observed orbit, by moving HAT-P-2 inward. Also due to its highly eccentric orbit and its orbit properties, the planet reaches the point of periastron passage 13 hours after the mid transit point T_0. This results in a steep change flux received from the host star and in a turbulent atmosphere, and the system is probably the most turbulent system known to date (Lewis et al. 2011 [34]).

The Template Since HAT-P-2 rotates with a vsini of about 20 km/s, the line profile is less smeared out than the WAPS-33 line profile. The same fit routine was used to obtain a sharp line template as for the WASP-33 data. This had the following side effect: shallow lines result in a relatively deep sharp line profile at the respective

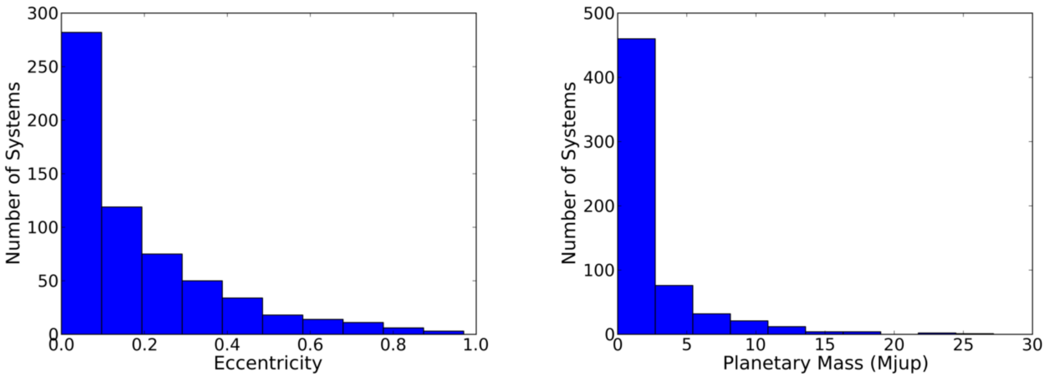

(a) Distribution of orbit eccentricities.

(b) Mass distribution in M_{Jup} of exoplanets.

FIGURE 4.5: According to exoplanetstable.org (Nov 2013).

wavelength position. This causes the reconstructed line profile to be deeper than the observed spectrum at these respective wavelength position. Furthermore the reconstructed broadening function seems to be multiplied by some scaling factor, since it was too flat and its wings did not fall to zero.

To investigate this, different approaches were tested. First all lines in the line list exceeding a certain width were flagged. Even though this solves some of the problems encountered with the sharp line template, the template does not fit well at the position of deep lines. The next test was instead of flagging the broad lines in the line list, the reduction of their width to the mean of all widths of the line list. The last test was to use the same width for all lines in the line list.

Comparing the last two approaches showed that there is a decrease in the computation time for the template when fixing the width to a universal value without resulting in a reduction of the goodness of the fit. To sum up it, is appropriate to use a priori defined fixed width for all lines for the HAT-2 data in order to obtain a good fitting template. As the linear limb darkening parameter 0.71 and for the stellar rotation velocity 21.3 km/s was used.

Orbital Solution To check whether the orbital parameters given by Loiellet et al. 2008 [35] are correct, I took the RV values from their Table 1 and also the ones from Bakos et al. (2007 [3]) from their Table 1 based on Keck and Lick data (the same data was also used by Loiellet et al. for their orbital solution). For the zero point correction the values by Loiellet et al. (see their Table 2) where applied. In a next step a MCMC fit was done to the data and the resulting best fit is within the error margins given by Loiellet et al. . The free fit parameters included the semimajor axis, the eccentricity and the argument of periastron passage ω.

To check if they accounted for the eccentricity during their modeling of the Rossiter-McLaughlin-Effect, I also did a MCMC fit using the analytic description by Ohta et al. 2005 [44]. The best fit solution results in a larger projected rotation velocity, vsini, of the host star than the spectroscopic obtained values (34 km/s instead of 21 km/s). This deviation is in agreement with the result Loilett et al. obtained during their fit without applying constraints on the parameter space of vsini. Using the literature value of Loilett et al. for vsini, the MCMC fit is in agreement with their results.

To sum up, both the result for the orbital solution and the Rossiter-McLaughlin-Effect could be reproduced. During the fit of the Rossiter-McLaughlin-Effect the eccentricity of the system was accounted for by Loilett et al.

There is a further paper by Pal et al. 2010 [45] that presents a refinement of the orbital parameters of the system. They have 14 additional Keck observations and also use the data from Loiellet et al. and Bakos et al. . Since they have more data available their fit should be an improvement of the orbital parameters. One reason for using the parameters from Loiellet et al. in the following is that I am not able to check their result as they do not state any zero point correction values. Another reason is that when fitting the residual map obtained for the HIRES data set for their orbital parameters the best fit did not remove the planetary signal for a reasonable value for the misalignment angle λ.

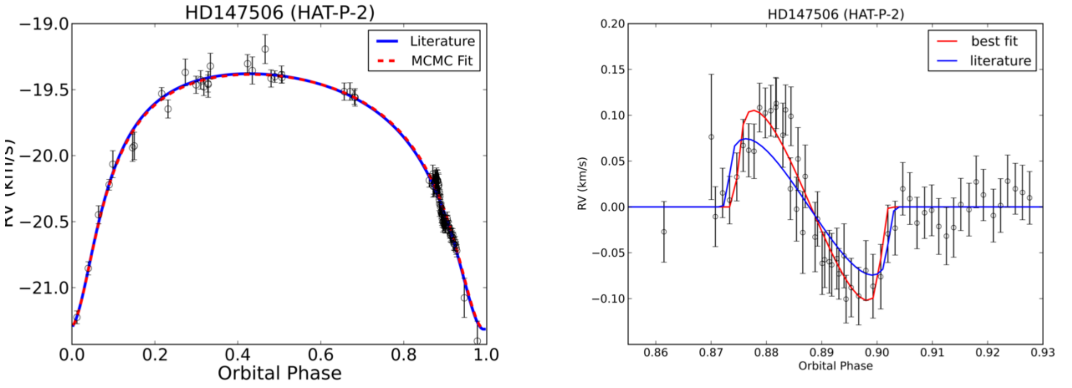

(a) Phase-folded radial velocity measurements of HAT-P-2 (Haute-Provence, Lick and Keck). Over plotted is the Keplerian orbit solution. For the blue curve the orbit parameters given by Loeillet et. al. where used. Red shows the solution if the mean of the MCMC fit values are taken as system parameters. Both literature values and the fit results are in perfect agreement.

(b) Phase-folded radial velocity measurements of HAT-P-2 (Haute-Provence, Lick and Keck) after subtracting the Keplerian orbit using literature values. For the blue curve, the orbit parameters given by Loeillet et. al. where used. Solid Red shows the solution if the mean of the MCMC fit values are taken as system parameters with the rotation of the host star fixed. Dashed Red shows the solution if the rotation velocity is set as free fit parameter.

Figure 4.6: HAT-P-2 radial velocity measurements.

4.2.1 SOPHIE

The Data The HAT-P-2 data set consists of data taken during the night of May 15, 2007, and another set taken on the night of June 11, 2007, at the 1.93m telescope of the Haute Provonce Observatory using the SOPHIE spectrograph (Section 3.1). The data was collected by the Sophie Exoplanet consortium (07A.PNP.CONS) and T. Mazeh program (07A.PNP.MAZE). They were first published by Loiellet et al. 2008 [35]. Even thought the raw images are available in the SOPHIE archive, no calibration files such as flat fields etc. are provided. Assuming the accuracy of their reduction is sufficient for my intended purpose, I used the pipeline reduced spectra which have merged orders. The data are not yet normalized. The spectra show a number of outliers. There are some structures visible, which are broad, up to 40 bins with 0.01 Å per bin. I removed the outliers as described in Section 3.3.3.
The data were divided into 80 Å sections to be normalized. The same approach as for the WASP-33 data set was chosen (Section 3.3.2). The second data set still exhibited some variations after the normalization that show sinusoidal behavior, about the length of an order. These are most probably a result of the merging of the orders during the reduction process. In order to remove these deformations, the following was done: In each of the 80 Å chunks containing 8000 bins, sub chunks consisting of 400 bins were defined (this value produced the best result and correction). For each chunk the mean flux value of the residual of each phase and the mean of all phases was calculated. In a next step, a cubic interpolation through these points was done (see Fig. 4.8). Dividing each phase by each resulting interpolation function, the strength of the variations was reduced. This is based on the assumption that in the residuals of the phases and the mean of all phases the variations are dominated deformations and not by statistical noise. A second effect that is apparent by visual inspection of the spectra, is that the data seem to have two different levels of strength of the variations and can be divided into two domains. It is unclear what causes this, since the first data set does not show this behavior. In the first data set there is also some sinusoidal variation present, but with a lower frequency and consistent over all phases of the observation. Since it is impossible to do the reduction of the raw images without calibration files, it is hard to say what could be the reason. Since activity can be cause of variations in the flux of a star, it was checked if there is an indication for a flare event. This was done by dividing the sum of the core emission of the Ca II H and K lines by the summed emission in a continuum region next to the Ca lines. As shown in Fig. 4.7, there is no indication that activity is the cause for the variations in the data. Other than the removal of the deformations by the above mentioned manner no further processing of the data was done.

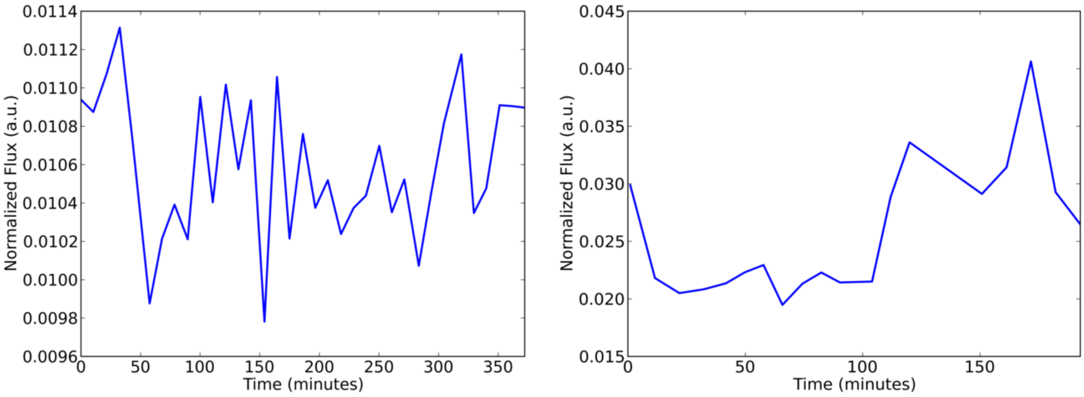

(a) First SOPHIE data set (b) Second SOPHIE data set

FIGURE 4.7: Check for signs of activity in the SOPHIE data using the Ca II H and K lines.

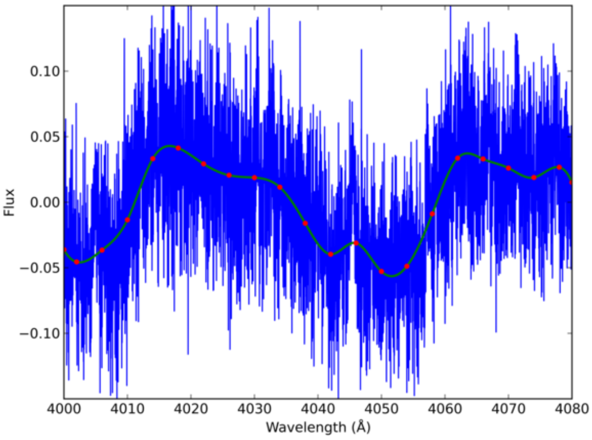

FIGURE 4.8: Residuen plot of the mean of all phases of the second HAT-P-2 SOPHIE data set and one of the phases. Over ploted is the cubic spline fit.

Bipolar Structure The LSD residuum maps for the first SOPHIE data set show some bipolar structure that, at first glance, could be caused by noise or other problems with the data set. This is a possibility, since with the second SOPHIE data set, LSD did not give reasonable results.

Using simulated transit data, the bipolar effect can be reproduced if for each phase the spectrum is Doppler shifted by an increasing small amount. The effect becomes visible at about a maximum shift of 1-2 % of the stellar rotation velocity. The cause for this Doppler shift in the case of the SOPHIE data becomes apparent by examining Fig. 4.6(a). The transit occurs at a phase where the stellar RV curve is steep: the star moves “fast” during the transit in regard to the observer. The reconstructed broadening functions are then shifted by some small value in the 0.4 to 0.2 km/s range in regard to their mean (which corresponds to the 1-2 %). Subtracting the mean of all broadening functions to obtain the LSD residual map causes this bipolar structure to appear.

To confirm the origin of the bipolar structure, a model was developed using Gaussian functions to model the shape of the structure. The center of each Gaussian was then shifted with a second order, time depend polynomial function. In parallel, a second Gaussian representing the planetary signal was subtracted from the model. This second Gaussian is shifted with the stellar RV below the planets center at each phase accordingly and also the amplitude is scaled with the respective linear limb darkening factor. From this a non-shifted Gaussian, representing the mean broadening function, was subtracted to model the bipolar structure. By subtracting this model from the simulated LSD map only the noise remains. To sum up, a simulation has shown that a Doppler shift can cause a bipolar structure, and it was possible to remove the bipolar structure through a model that simulates a Doppler shift of the reconstructed profile.

Since the relative shift causes the planetary signal to be offset in the LSD residual maps, there are two ways to deal with this:

A. Calculate the LSD map and correct the shift afterwards.

B. Take the shift into account when creating the template for LSD (for each phase this results in one template).

A. would require interpolating the broadening function to a higher resolution since the effect is at sub-bin level. This is why B. was chosen as the preferred method. Therefore for each phase, a template was created that takes this Doppler shift into account. To be able to calculate the strength of the Doppler shift, the orbital solution was derived from the SOPHIE data set.

4.2.1.1 Direct Profile Modeling

Even though the WASP-33 data set showed that the direct profile modeling approach can reproduce the literature values, it also showed that the method is not usable for a system without a priori knowledge of the planetary orbit configuration. A simulation of the HAT-P-2 system has shown that the direct profile modeling approach is not able to recover the input orbital parameters in the case of this system (Section 2.1). To verify this, and since the first LSD results for HAT-P-2 looked promising, a direct profile modeling was also done to both data sets available from the SOPHIE spectrograph (Fig. 4.9). The method again, like in the simulation, shows a local minimum which is inconsistent with the results from LSD (Fig. 4.9), and therefore questionable. The value for the misalignment angle λ would result in a transit that is almost in parallel to the rotation axis. The fit prefers values around 90° to 100°, and this is consistent for the majority of the 80 Å long spectral chunks the merged spectra were divided into. The minimum is therefore no artifact, a problem of the template in a single wavelength section, or caused by noise.

Because both data sets do not cover a complete transit, it was tested if adding the resulting reduced χ^2 maps of each data set would result in a local minimum around literature values. However this is apparently not the case (Fig. 4.9(c)).

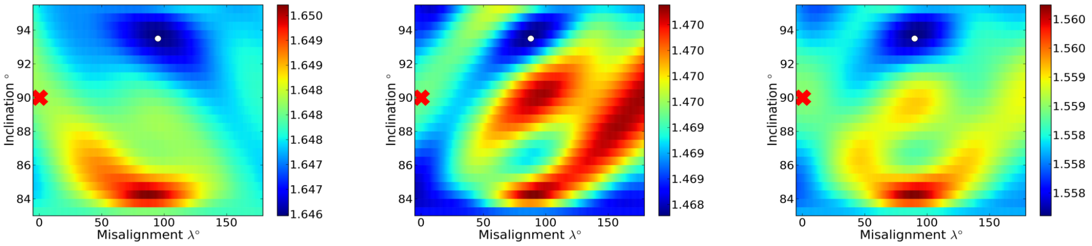

(a) First SOPHIE data set covering the last 2/3 of the transit.

(b) Second SOPHIE data set covering the first 2/3 of the transit.

(c) Add up of the resulting reduced χ^2 maps of the first and the second SOPHIE data set.

FIGURE 4.9: Reduced χ^2 maps for the HAT-P-2 SOPHIE data set. Only the inclination and the misalignment angle λ were varied for each phase. The red cross marks the literature values. The white circle marks the position of the lowest reduced χ^2 value.

4.2.1.2 Least Squares Deconvolution

For computation time reasons and also to reduce the number of free parameters that have to be fitted at once the spectra were divided in 20 Å regions, resulting in each region having its own best fit stellar template. This makes it possible to check in each region the resulting broadening function for deformations and decide whether some wavelength regions have to be flagged as not usable.

One phenomenon that showed up is that the resulting broadening function has wings and the peak is too sharp to fit the theoretical broadening function based on rotational broadening [1]. Fitting this broadening function to extract the host star's rotational velocity as done with the WASP-33 data set is therefore impossible.

Apart from these problems for the first SOPHIE data set LSD produces a visible planetary track (Fig. 4.10(a)). There is a bi-polar structure, which is caused by a RV change during the transit (Fig. 4.6(a)).

As mentioned in the Section 4.2.1, the second data set shows deformations of each phase in regard to the mean of all phases following the normalization. The first attempt for LSD showed no planetary track and also there seemed to be two separate sections in the map (Fig. 4.10(b)). The broadening functions of each phase are either above or below the mean broadening function. The reduced data can also be divided into two domains. One domain shows stronger variations than the other. It was assumed that these variations have no effect on LSD and the reconstructed broadening function. In order to check if the variations are the cause for LSD to fail, the strength of the

---

[1] The wavelength range has been converted into a log-scale range where each bin is corresponds to a RV of 1 km/s

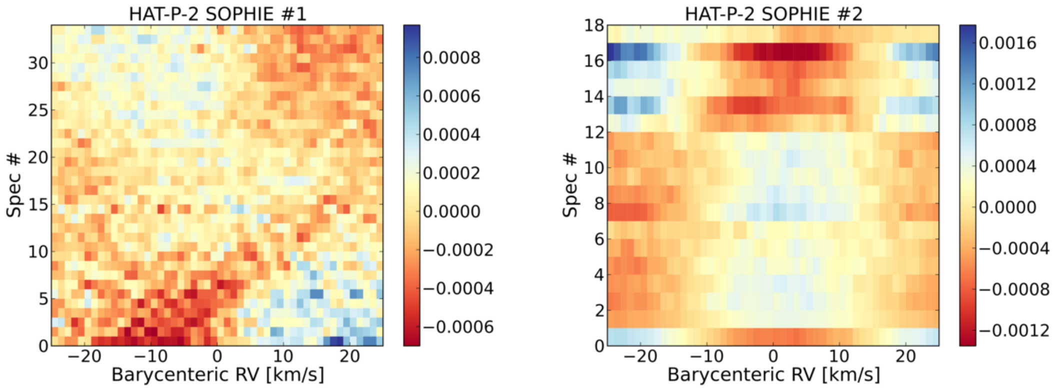

(a) First SOPHIE data set

(b) Second SOPHIE data set

FIGURE 4.10: Calculated LSD residual maps for each of the two SOPHIE data sets. Both were calculated using a template based on a radial velocity of 20 km/s. As the right figure clearly shows LSD fails to reconstruct a meaningful profile for the second data set.

variations were reduced by applying a spline fit to the residuals of each phase and the mean of all phases (Section 4.2.1). Comparing the result with and without the correction showed that it is indeed the case that LSD is insensitive to these variations and the failure is not caused by the variations. As a last attempt, the reconstructed broadening functions were divided into two parts. The LSD residuals map created with the mean of each part respectively, did not show any improvement and no planetary track becomes visible.

Since it is impossible to do the data reduction (missing calibrations files), it cannot be checked if the cause of the LSD failure is in the reduction process. It was decided that no further work should be invested into the second data set.

As mentioned in the paragraph “Bipolar Structure”, if a fixed value for the radial velocity for each phase is used, a bipolar structure appears due to the fact that the radial velocity of the star changes during the transit by a value of about 0.4 km/s. To counter this, for each phase a sharp-line template was calculated accounting for the radial velocity shift calculated using the orbital solution (Section 4.2).

To get the best fit values a MCMC fit was carried out using 500,000 steps. Since the simulation in Section 2.2 had shown that it is impossible to recover the eccentricity and the argument of periastron passage ω, only the inclination and the misalignment angle λ where set as free fit parameters. The resulting best fit model (Fig. 4.11(b)) was then subtracted from the reconstruction (Fig. 4.11(a)). Clearly, the planetary track vanishes, only noise remains (Fig. 4.11(c)).

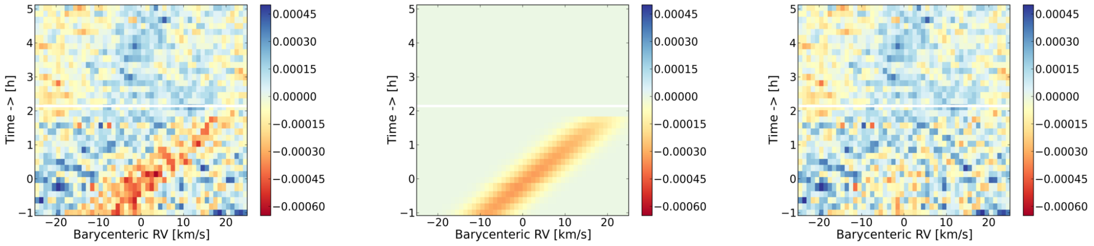

(a) First SOPHIE data set including orbital motion correction

(b) The best fit planetary transit model using MCMC

(c) Subtracting the planetary transit model from the data

FIGURE 4.11: LSD residual maps calculated for the First SOPHIE HAT-P-2 data set.

4.2.2 HIRES

The Data In order to assess the possibility to use HIRES data contaminated with an Iodine cell, data taken during the night of June 6 to 7 2006 of HAT-P-2 were analyzed (Winn et al. 2007 [67]).

HIRES has three CCDs. In the wavelength range of the first CCD there are no Iodine lines present and these data was then chosen for further analysis. The third CCD has also no Iodine lines present but the normalization was not stable, when comparing different phases of the observation, so no further work was done with CCD three. For the second CCD in the wavelength range of the Iodine cell the data are missing from the archive.

Even though there are calibration files provided, a first attempt was done with the already reduced data that is the result of their automatic pipeline. Since the orders are not merged the same approach as for the WASP-33 data set was applied, working with each order separately.

The data were checked for outliers and no significant signal was found. The same approach for the normalization and for obtaining a template was used as described in Section 3.3.2 and Section 3.3.4. There is one important difference between SOPHIE and HIRES data sets: the HIRES wavelength range is in vacuum and the SOPHIE in air. This has been accounted for the template used for the normalization as well as for the line list used for the multi-Gaussian fit. Also each phase of each order has its own wavelength range with different start and end values.

Bipolar Structure As mentioned in Section 4.2.1 there should be the presence of a bipolar structure due to the change in the radial velocity during the transit. For the SOPHIE data set using the global orbital solution to account for this change was sufficient to remove the bipolar structure. This was not the case for the HIRES data. The bipolar structure is still present even after accounting for the orbital solution. A cross-correlation with a stellar template revealed a strange behavior of the wavelength calibration. The first troubling result was that each order has a different offset in the radial velocity, although the general form of the curve remains the same. And the second that at about mid-transit phase there is a clear jump in the RV obtained using the cross-correlation.

In comparison to the curve from the global orbital solution the deformation of the radial velocity curves seem to be of instrumental origin since the planetary transit cannot be the cause for this behavior. Since there are no iodine lines present in CCD one, the wavelength solution can be unstable and this could be the cause for the observed phenomena. Doing a cross-correlation with the third CCD reveals the same curvature.

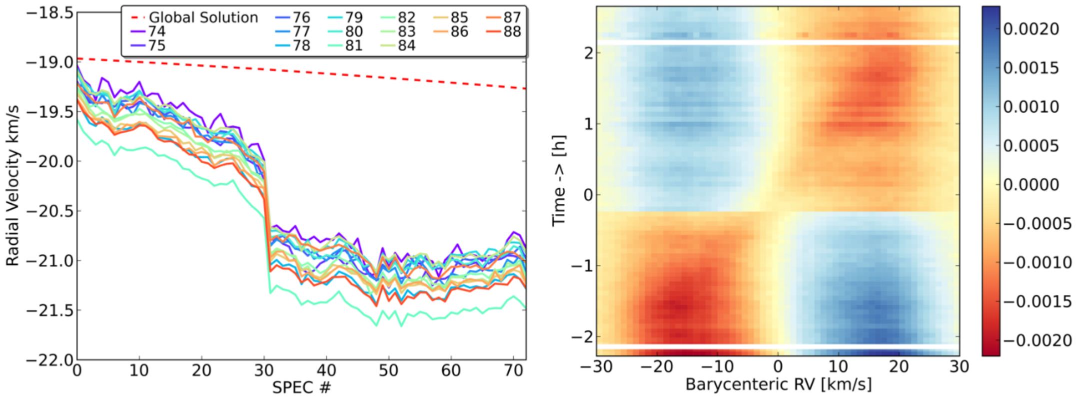

(a) RV shift of each order calculated using a cross-correlation with a stellar template..

(b) First residuals map calculated using LSD without accounting for the RV shift.

4.2.2.1 Direct Profile Modeling

As with the SOPHIE data set also a reduced χ^2 map was calculated. Again the lowest reduced χ^2 value is in a region that is in stark disagreement with the literature values, and the orbital parameters extracted using LSD in Section 4.2.1.2 and Section 4.2.2.2. The calculation was done to check if the method could work with a data set that has higher spectral resolution and a better S/N ratio ($\approx 60-80$ vs. $\approx 100-150$) then the SOPHIE data set. Again the results appears to be highly questionable, however.

4.2.2.2 Least Squares Deconvolution

The HIRES data set proved to be challenging since the wavelength solution of the HIRES pipeline-reduced spectra is not stable. A correction had to be applied in order to remove any artefacts caused by the unstable wavelength solution, creating sharp line templates for each phase of each order respectively (Section 4.2.2).

Taking into account the correction, the final solution shows a strong planetary signal (Fig. 4.13(a)). The signal was fitted using MCMC with the model as described in

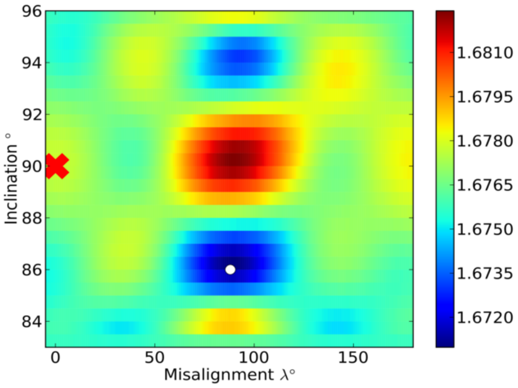

FIGURE 4.12: Reduced χ^2 map for the HAT-P-2 Hires data set. The red cross marks the position of the literature values. The white dot marks the lowest reduced χ^2 value.

Section 2.2 using 500,000 steps. As with the SOPHIE data, only the orbital inclination i and the misaligned angle λ where set as free fit parameters. Subtracting the best fit model from the reconstruction, the planetary signal vanishes and only the noise remains. The result is in good agreement with literature values, especially for the misalignment angle λ the result point towards a almost alignet system (Table 4.2).

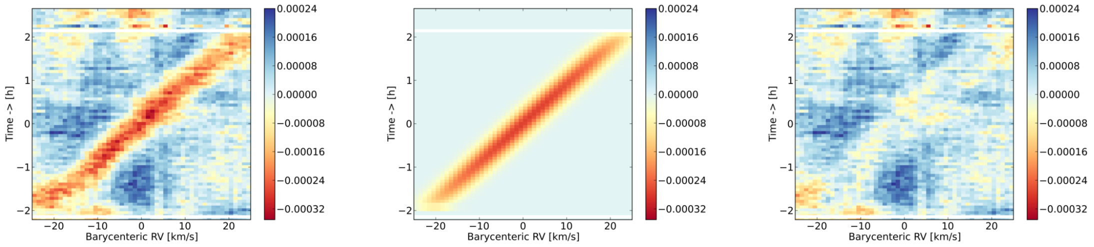

(a) The resulting residual map for the HAT-P-2 HIRES observation

(b) The best fit planetary transit model using MCMC

(c) Subtracting the planetary transit model from the data

FIGURE 4.13: LSD residual map calculated for the HIRES HAT-P-2 data set.

4.2.3 Discussion

I analyzed two independent data sets from two different telescopes and spectrographs. The problems with the second SOPHIE data set and the unreliable wavelength solution of the HIRES data show that a user has always to be careful. In the case of the SOPHIE data there exists no possibility to do the reduction by the user. The user has to trust the data and that all the flaws inside the data have been found. I was able to fix the wavelength solution for the HIRES data, and therefore doing the reduction was not necessary. But this is not always the case as the XO-3b HIRES data set has shown (Section 5.3).

The DPM approach failed for both data sets and the cause for this is unknown. A simulation of the system has already shown that there is some fundamental problem with the method. As mentioned before the only hint that could possibly point in the right direction is the stellar template that is used. It is impossible to get a perfect fitting template and the reconstruction of deformation caused by a planetary transit seems to strongly depend on this. For HAT-P-2 an independent confirmation of the result from LSD is therefore impossible as with the WASP-33 data.

In the case of the SOPHIE data, the reconstructed orbital parameters differ from the ones obtained using the Rossiter-McLaughlin-Effect. The data itself has some problems as the fit of the Rossiter-McLaughlin-Effect prefers a higher stellar rotational velocity than the spectroscopically obtained one. Also there is no complete transit available since the second SOPHIE data set that covers the other half of the transit was not usable. The S/N of the data is worth then the one of the HIRES data set, and, as a result, the planetary signature is more smeared out. This, in the combination with the missing start transit points, could result in the reconstruction of wrong orbital parameters. Ingress and egress phase of a transit are important as they have a influence on the reconstructed orbital inclination angle i. The conclusion is that without this phases of the orbit the reconstructed parameters cannot be trusted.

In the case of the HIRES data, the reconstruction shows a strong planetary signal. The transit starts and ends at the position of literature values derived form photometry. In their paper, Albrecht et al. did a re-analysis of the same data by using the anomaly and in their conclusion they suggest the use of LSD to recover the orbital parameters is more reliable. The smaller error bars I obtained also point in this direction (Table 4.2).

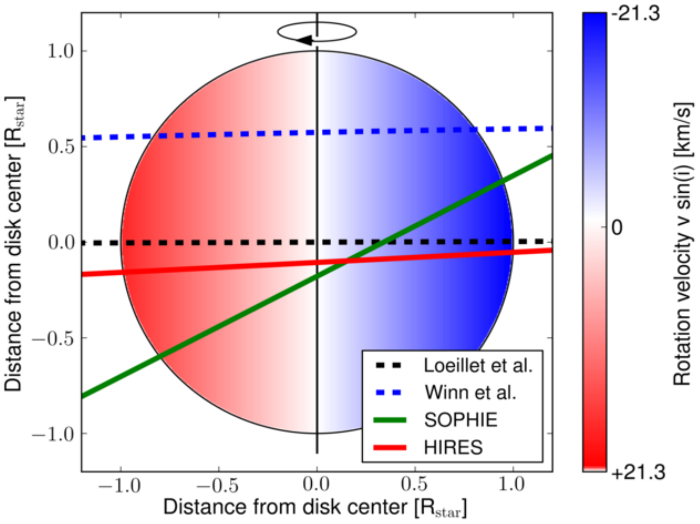

FIGURE 4.14: Visualisation of the planetary track on the stellar surface for the literature values by Loiellet et al., Winn et al., Albrecht et al. and the results from this work's LSD reconstruction of the SOPHIE and HIRES data. The track for Winn et al. is for the lower value for the inclination.

TABLE 4.2: HAT-P-2 system parameters by Loiellet et al. 2008 [35], Winn et al. 2007 [67], Pal et al. 2010 [45], Albrecht et al. 2012 [1] and this work.

Parameter (Unit)	Loeillet	Winn	Pal	Albrecht	This work	
					SOPHIE	HIRES
Orbital period (d)	5.63341 ± 0.00013	5.63341 ± 0.00013	5.6334729 ± 0.0000061	-/-	-/-	-/-
Orbital inclination, i (deg)	$90.0^{+0.85}_{-0.93}$	> 86.8 (95% conf.)	$86.72^{+1.12}_{-0.87}$	-/-	$90.8839^{+0.5095}_{-0.4578}$	$90.5934^{+0.6614}_{-0.7261}$
Misalignment, λ (deg)	$0.2^{+12.2}_{-12.5}$	1.2 ± 13.4	-/-	9 ± 5	$27.724^{+6.500}_{-6.937}$	$3.0112^{+3.9095}_{-1.6309}$
Stellar radius ($R_\odot$)	$1.416^{+0.04}_{-0.062}$	1.48 ± 0.05	$1.64^{+0.09}_{-0.08}$		-/-	-/-
Planet Radius (R_{Jup})	$0.951^{+0.039}_{-0.053}$	0.98 ± 0.04	$1.157^{+0.073}_{-0.062}$	-/-	-/-	-/-
eccentricity e	$0.5163^{+0.0025}_{-0.023}$	0.501 ± 0.007	0.5171 ± 0.0033	-/-	-/-	-/-
Orbital major semi-axis, a (AU)	0.02555 ± 0.00017	-/-	0.06878 ± 0.00068	-/-	-/-	-/-
Stellar rotation, vsini (km/s)	21.3 ± 1.3	19.6 ± 1.0	20.8 ± 0.3	19.5 ± 1.4		

Chapter 5

Summary

It has been a challenge to work with data from different spectrographs and the direct profile modeling (DPM) proved to be unreliable. Nevertheless in the course of this thesis it has been successfully shown that the approach first applied by Collier-Cameron et al. "Line Profile Tomography" 2010 [9] can be applied to different systems and differing data sets without changing the basic principle behind the method.

5.1 Direct Profile Modeling

The direct profile modeling approach gave some mixed results. Theoretically it should result in better constrained orbital parameters then the approaches that fit the Rossiter-McLaughlin-Effect. The planetary transit actually results in a deformation of the line profile not a radial velocity shift. The reconstructed orbital parameters also depend on how accurately the modeling of the anomaly represents the physics that cause the effect.

In the course of the development of the method, a simulation of two different systems has shown that the model is not stable in the reconstruction of the input parameters, if the same steps as with real data are done. The approach works in case of a perfect fitting template but as soon as there is some deviation the method starts to have problems recovering the input values. There is the indication that the failure is related to the quality of the template, but it is unknown whether this depends on some other system parameter, if there exists a lower boundary condition for a parameter such as the planet star size ratio.

In the case of the WASP-33 system it was shown that the method is not usable standalone. Without prior knowledge of the system parameters, no best fit value can be returned. For observational data as for a simulation the best fit value was for no planetary transit signal present in the data. Still there are local minima at a reasonable position. The error on the orbital inclination i and the misalignment angle λ is lower then the one derived from the LSD reconstruction. This is an expected behavior for a model with fewer degrees of freedom.

In the case of the HAT-P-2 system the direct profile modeling failed for both data sets that were analyzed and recovered unreasonable orbit parameters. Even a simulation of the system did not shed light on the cause for this failure. In a simulation the input parameters are known. Therefore it is unlikely that the orbital parameters recovered for observational data with complementary methods, such as the modeling of the RV anomaly or Line Profile Tomography, are wrong.

Systematic effects render the method inapplicable or - at least - impede the application.

5.2 Least Squares Deconvolution

LSD showed to be a stable way to extract orbital system parameters from the data. The most challenging part of the method is to get a good fitting template. When the data is already reduced and have no artefacts that have to be corrected for, the final result can be obtained within a week. This includes the normalization, the template fitting, the application of LSD and the planetary model fit. The planetary model is simple, Gaussian shaped, and includes the rotational velocity of the host star, the limb darkening, the size ratio of the planet / host star, the semi-mayor axis and the orbital period of the planet. The template creation is independent of this step and the correct modeling of the physics of the host star is not part of the planetary model.

The correction of the radial velocity present in the data has proven to be crucial for LSD to work correctly. A simulation has shown that the orbital parameters depend on the correct determination of the RV shift of the spectra. In case of the HAT-P-2 system an error of 1 km/s results in a change of the best fit misalignment angle λ of about 3°. Therefore the method can result in wrong orbital parameters if the RV shift is not correctly accounted for. It is therefore advisable to do a cross-correlation with each spectrum respectively to get the correction factor, even with data from a stable spectrograph as HIRES.

The analysis of the SOPHIE data also showed that it is important to have the complete transit phase available, or at least the ingress and egress phase should have been observed.

A comparison between the steps needed for the reconstruction to work in case of LSD to the analytic formulae by Ohta et al. 2005 [44] or the rather sophisticated one by Hirano et al. 2011 [27] clearly shows an advantage of LSD. As already mentioned in Section 1.2 if the spectral lines show broadening the formulae by Otha et al. need time consuming a priori numerical modeling to counter the discrepancy between the first moment and the value obtained from a cross-correlation. To improve this Hirano et al. directly modeled the effect of the different broadening mechanisms that change the strength of the observed anomalous RV shift.

Therefore the correction is applied in the model fit. The influence of each of these corrections on the final solution has to be accounted for. A model that does not need these corrections is simpler and less prone to have systematic errors. Further Ohta et al. and Hirano et al. both have the downside that the position of the planet in the profile and the strength of anomaly is fitted at the same time, whereas when using LSD only the position is fitted.

In addition an advantage of LSD is that it works in the case of fast rotators - like WASP-33 - where the modeling of the Rossiter-McLaughlin-Effect is inapplicable.

5.3 Future Applications

Further work has been done for two systems in the course of this thesis: WASP-7 and X0-3. The reason they do not appear in the main part of this thesis is that these are only preliminary result, so more work has to be done in the near future.

For WASP-7 my proposal “Differential rotation of WASP-7” (ESO VLT/ UVES 91CfP) was successfully accepted, and the observation was done in the night of 31.08.2013 to 01.09.2013 in visitor mode by me. The first reconstruction for the WASP-7 data set using LSD showed some bipolar structure (Fig. 5.1). Doing a cross-correlation with a stellar template revealed that the WASP-7 data show a time dependent wavelength shift that seems to be related to the trend of the pressure value inside the spectrograph. As with the HAT-P-2 HIRES data for each spectrum a template was created accounting for this shift. Currently the noise in the residuals map has the same magnitude as the transit bump of WASP-33b even when taking into account the RV shift. Due to the smaller planetary size, the planetary signal should be weaker than the one from WASP-33b. Therefore no planetary track is visible yet.

Since the UVES pipeline produces spectra with merged orders there might be a varying wavelength dependent RV shift for each order hidden in the data. A next step will be to take a look at each order separately and doing a cross-correlation respectively to get the correct value of the RV shift.

In the case of X0-3 there is high resolution data available from HIRES, SOPHIE, and SUBARU. Since the code for obtaining the normalization and the template was already set up, a short analysis of the HIRES data was done. The same applies as for the HAT-P-2 data: each order shows a time dependent wavelength shift. Another problem is that the pipeline-reduced data show some artefacts in some phases of different orders. The first attempt that accounted for the RV shift, and flags the spectra with obvious flaws, shows a bump that could be the planetary transit signal (Fig. 5.2(a)). In the map some phases were additionally flagged after the reconstruction of the broadening function due to deformations. A visual inspection of each order of these phases did not reveal the cause for the observed phenomena. There is also some structure present

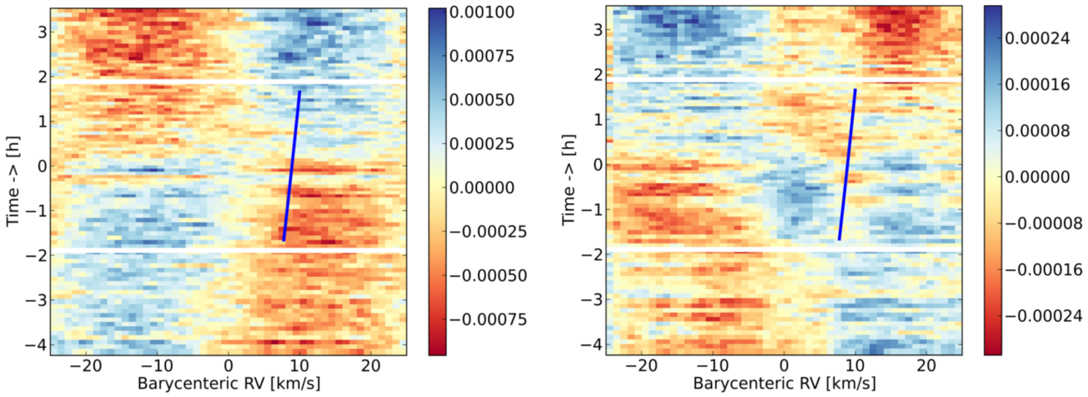

(a) First attempt to reconstruct the planetary transit signature for the WASP-7 data.

(b) Second attempt to reconstruct the planetary transit signature for the WASP-7 data, after applying the RV correction for each template.

FIGURE 5.1: In blue is the planetary track according to literature values. The horizontal white lines marks the begin and end of the transit respectively. The level of noise is reduced when accounting for the RV shift present in the spectra. Still there is some structure and the planetary track is hidden in the noise.

in the reconstruction. It is therefore advisable as next step to do a reduction of the raw data, not rely on the already reduced data in the archive and to proof that there really is a planetary signal and not some deformation due to the problematic data. A 500,000 steps MCMC fit carried out to the residual map using the planetary model did not result in a complete removal of the bump at the position of the best fit values (Fig. 5.2(c)). Still the reconstructed orbital parameters for the orbital inclination $i = 86.0391^\circ\ ^{+0.5406}_{-0.7260}$ and the misalignment angle $\lambda = 35.6676^\circ\ ^{+7.0817}_{-7.7310}$ are comparable to known literature values by Winn et al. (84.20° $\pm\,0.54$ 2008 [65]; $\lambda = 37.3^\circ\ \pm 3.7$ 2009 [66]). The data are therefore usable for the method and it is worth to invest additional time.

It would also be interesting to take a look at the XO-3 SOPHIE data, in order to check whether there is a fundamental problem with the data from this spectrograph when

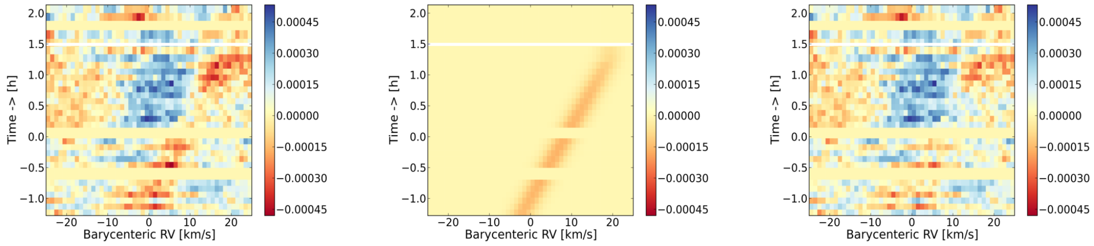

(a) The resulting residual map for the XO-3 HIRES observation

(b) The best fit planetary transit model using MCMC

(c) Subtracting the planetary transit model from the data

FIGURE 5.2: LSD residual map calculated for the HIRES XO-3 dataset. The white lines mark the start and end of the transit according to Winn et al.

using LSD. Also there is further high-resolution data available from a different spectrograph (Subaru /HDS), so a comparison between three data sets would be possible. Another interesting test case would be the HAT-P-34 HIRES data. There the mid-transit phase is missing. With these data the behavior of LSD with incomplete transits that still cover the ingress and egress phase could be tested. This variant could be tested by leaving out some data in already existing data sets but then a comparison to how complementary methods react to incomplete data is impossible. It has been confirmed in the course of this thesis that LSD can improve the result with a complete transit but it has to be shown if this is also true with a missing mid-transit phase.
There are also other interesting targets HAT-P-41b, KELT-1b and WASP-79b, where high resolution spectroscopic data is not available at the moment.

5.4 Outlook

The direct profile modeling approach is partly working for one system (WASP-33) and failed for a second one (HAT-P-2). Since the cause is unknown and the reconstruction using LSD proved to be fast and stable, any further work in this direction has a big question mark. DPM shows lower statistical errors but there is an unknown level of systematic errors, such as the incomplete template, and as the simulation has shown has problems recovering the exact input values. LSD on the other hand recovers the input values and also works in the case of a system where DPM failed.
As already mentioned in the previous section “Future Applications” there are new targets available (HAT-P-41b, KELT-1b and WASP-79b), there is still data to be analyzed in the archives (HAT-P-34b and XO-3b) and I have my own unpublished data (WASP-7b). After the start of this thesis the candidate list of usable systems increased by two systems, and this list will probably increase even further in the near future.
Collier-Cameron et al. 2010 [9] used a variant of LSD for HD189733, a slow rotator with a stellar rotation velocity of 3.10 ± 0.03 km/s, so an expansion in this direction is possible. This would result in a much larger candidates list. Slow rotators are more challenging in obtaining a correct template since the final reconstruction of the broadening function is not dominated by rotational broadening only. I had access to our own data of the same system but was not able to do a complete analysis in the course of this thesis (“Scanning both outer atmospheres of the exoplanetary system HD 189733” ESO VLT / UVES 89Cfp).
With the new instruments available in the near future such as the Extremely Large Telescope (ELT), the shortcomings of the modeling of the Rossiter-McLaughlin effect will become even more pronounced, that the modeling of the planetary position in

the line profile and the strength of the anomalous RV shift is fitted at the same time. The resolving of the planetary transit signal or “bump” will improve and therefore the correction already needed - in order for the modeling to work - might not be sufficient any more to recover the correct orbital parameters.

List of Figures

List of Tables

Appendix A

Tables

Table A.1: Radial Velocity (RV) values for HAT-P-2. The data includes the barycentric correction and has been shifted to account for different zero points. OHP stands for Haute-Provence Observatory (see 3.1).

BJD (-2400000) days	**RV** (kms^{-1})	**Uncert.** (kms^{-1})	**Observatory**
54227.5016	-19.4014	0.0088	OHP
54227.6000	-19.4082	0.0065	OHP
54228.5842	-19.5581	0.0188	OHP
54229.5993	-20.1874	0.0161	OHP
54230.4475	-21.2249	0.0141	OHP
54230.6029	-20.8536	0.0148	OHP
54231.5987	-19.5311	0.0121	OHP
54235.3466	-20.1916	0.0156	OHP
54235.3538	-20.2318	0.0180	OHP
54235.3615	-20.3008	0.0167	OHP
54235.3692	-20.2790	0.0173	OHP
54235.3765	-20.3083	0.0172	OHP
54235.3866	-20.3889	0.0209	OHP
54235.3938	-20.4280	0.0171	OHP
54235.4011	-20.4370	0.0173	OHP
54235.4088	-20.4450	0.0163	OHP

Continued on next page

Table A.1 – continued from previous page

BJD (-2400000) days	**RV (kms^{-1})**	**Uncert. (kms^{-1})**	**Observatory**
54235.4161	-20.4530	0.0180	OHP
54235.4234	-20.4987	0.0150	OHP
54235.4310	-20.5197	0.0144	OHP
54235.4383	-20.5032	0.0157	OHP
54235.4456	-20.5318	0.0178	OHP
54235.4535	-20.5340	0.0182	OHP
54235.4608	-20.4990	0.0143	OHP
54235.4681	-20.5047	0.0124	OHP
54235.4759	-20.4747	0.0117	OHP
54235.4831	-20.4974	0.0113	OHP
54235.4904	-20.5364	0.0111	OHP
54235.4981	-20.5384	0.0111	OHP
54235.5054	-20.5484	0.0108	OHP
54235.5126	-20.5785	0.0135	OHP
54235.5204	-20.6029	0.0142	OHP
54235.5277	-20.6066	0.0153	OHP
54235.5350	-20.5946	0.0115	OHP
54235.5434	-20.6155	0.0118	OHP
54235.5507	-20.5987	0.0113	OHP
54235.5580	-20.6266	0.0110	OHP
54235.5682	-20.6683	0.0119	OHP
54235.5755	-20.6712	0.0123	OHP
54235.5827	-20.6585	0.0115	OHP
54235.5905	-20.6819	0.0108	OHP
54235.5978	-20.7002	0.0128	OHP
54235.6051	-20.7205	0.0117	OHP

Continued on next page

Table A.1 – continued from previous page

BJD (-2400000) days	**RV** (kms^{-1})	**Uncert.** (kms^{-1})	**Observatory**
54236.5190	-20.2207	0.0056	OHP
54263.4521	-20.2320	0.0157	OHP
54263.4594	-20.2150	0.0100	OHP
54263.4666	-20.2318	0.0089	OHP
54263.4739	-20.2157	0.0092	OHP
54263.4804	-20.1896	0.0114	OHP
54263.4860	-20.2020	0.0120	OHP
54263.4915	-20.2102	0.0128	OHP
54263.4971	-20.1699	0.0096	OHP
54263.5030	-20.1835	0.0102	OHP
54263.5086	-20.1885	0.0108	OHP
54263.5141	-20.1880	0.0104	OHP
54263.5236	-20.2080	0.0103	OHP
54263.5291	-20.2225	0.0151	OHP
54263.5347	-20.3316	0.0179	OHP
54263.5411	-20.3661	0.0277	OHP
54263.5561	-20.3727	0.0127	OHP
54263.5634	-20.4279	0.0133	OHP
54263.5706	-20.4439	0.0173	OHP
54263.5779	-20.4647	0.0107	OHP
54263.5852	-20.5033	0.0091	OHP
53981.7775	-20.1400	0.0084	Keck
53982.8717	-20.4481	0.0085	Keck
53983.8148	-19.6469	0.0088	Keck
53984.8950	-19.3034	0.0086	Keck
54023.6915	-19.4262	0.0099	Keck

Continued on next page

Table A.1 – continued from previous page

BJD (-2400000) days	**RV (kms^{-1})**	**Uncert. (kms^{-1})**	**Observatory**
54186.9982	-19.4638	0.0055	Keck
54187.1041	-19.4794	0.0057	Keck
54187.1599	-19.4539	0.0053	Keck
54188.0169	-19.4155	0.0053	Keck
54188.1596	-19.3858	0.0055	Keck
54189.0104	-19.5151	0.0057	Keck
54189.0889	-19.5143	0.0062	Keck
54189.1577	-19.5588	0.0061	Keck
54168.9679	-20.0647	0.0421	Lick
54169.9519	-19.3696	0.0413	Lick
54170.8619	-19.3552	0.0426	Lick
54171.0365	-19.1929	0.0496	Lick
54218.8081	-21.0772	0.0883	Lick
54218.9856	-21.4046	0.0908	Lick
54219.9373	-19.9402	0.0439	Lick
54219.9600	-19.9268	0.0439	Lick
54220.9641	-19.4604	0.0384	Lick
54220.9934	-19.3213	0.0371	Lick

Appendix B

Proposals

After having successfully applied the LSD method to WASP-33b, I found myself in the comfortable position to set up a proposal for the period 91 call for proposal of ESO to obtain a new data set with properties designed for my purpose. I did a possible candidate search and the final list included HAT-P-34, HAT-P-41 and WASP-7. As already discussed in Chapter 3 "The Super-WASP discovered system WASP-7b offers not only the possibility to use the direct profile modeling approach and LSD, but also to measure differential rotation. The scientific case for observations is much stronger and we decided to propose for WASP-7". My Co-investigators S. Czesla and K. F. Huber used my transit code to simulate the effect of differential rotation on the position of the planetary transit signal in the line profile (Fig. 1 D of the proposal) and to assess the possibility to successfully measure differential rotation using the spectral resolution of UVES (Fig. 1 E of the proposal). I verified that the planetary orbit can be recovered using the proposed instrumental set-up. The proposal was accepted and I hereby thank my Co-Is S. Czesla, K. F. Huber, U. Wolter and J. H. M. M. Schmitt for supporting me as principle investigator and making this possible. The observation was carried out in the night of 31.08.2013 to 01.09.2013 in visitor mode by me.

European Organisation for Astronomical Research in the Southern Hemisphere

OBSERVING PROGRAMMES OFFICE • Karl-Schwarzschild-Straße 2 • D-85748 Garching bei München • e-mail: opo@eso.org • Tel.: +49 89 320 06473

APPLICATION FOR OBSERVING TIME PERIOD: **91A**

Important Notice:

By submitting this proposal, the PI takes full responsibility for the content of the proposal, in particular with regard to the names of CoIs and the agreement to act according to the ESO policy and regulations, should observing time be granted.

1. Title Category: **C–7**

Differential rotation of WASP-7 revealed by its transiting planet

2. Abstract / Total Time Requested

Total Amount of Time:

We propose to measure surface differential rotation (DR) on the planet host-star WASP-7 by means of transit spectroscopy and Fourier analysis. WASP-7 is a bright, fast rotating ($v\sin(i) = 17$ km/s) planet host-star of spectral type F5V, transited by a hot Jupiter in a massively oblique orbit. During transit, WASP-7b traverses its host star from lowest to highest latitudes and thereby "scans" nearly the entire latitudinal range of stellar rotational velocity. Based on high-quality transit spectra, we will reconstruct the time-dependent, average line profile using the least-squares deconvolution technique. This enables us to measure DR by following the planet's path across the host star. Additionally, the fast rotation allows to determine DR through Fourier analysis. The measurements will—for the first time—allow to determine stellar differential rotation using a planet and provide the unique opportunity to compare the result to the values *independently* obtained with the Fourier technique.

3. Run	Period	Instrument	Time	Month	Moon	Seeing	Sky	Mode	Type
A	91	UVES	1n	sep	n	1.0	CLR	v	

4. Number of nights/hours	Telescope(s)	Amount of time
a) already awarded to this project:		
b) still required to complete this project:		

5. Special remarks:

This observation can only be carried out in the night Aug. 31 - Sep 2, 2013.

6. Principal Investigator: Fabian Pfeifer

6a. Co-investigators:

S.	Czesla	1311
K.F.	Huber	1311
U.	Wolter	1311
J.H.M.M	Schmitt	1311

7. Description of the proposed programme

A – Scientific Rationale: Over the last years, hundreds of extrasolar planetary systems have been discovered, some of which with properties drastically different from those of our Solar System planets. Surprisingly, Jovian planets—many of them transiting—were found in close proximity to their host stars in virtually all conceivable orbit configurations. While some transiting hot Jupiters (e.g., HD 189733) show "normal" orbits with orbital and stellar rotation axes aligned, many counterexamples are known like the retrograde orbit of WASP-33b and the extremely oblique orbit of WASP-7b, which transits its host star almost from pole to pole (cf., Fig. 1 A). This special geometry provides a key to study latitudinal structure on planet-host stars, most notably, differential rotation (DR).

The Sun shows clear DR: While the solar equator rotates with a period of 25 d, the pole completes a full rotation only within 35 d. DR arises from the interplay of convective motions and Coriolis forces in all stars with outer convective envelopes (e.g., Küker et al. 2011, A&A, 530). Measurements of stellar DR are difficult: On slow rotators with spots, DR can usually only be measured using photometric spot-tracking, a method prone to produce ambiguous results; for fast rotators Doppler Imaging and the "Fourier method" can be applied. The latter relies on a Fourier decomposition of the stellar line profile (e.g., Ammler-von Eiff and Reiners 2012, A&A, 542, for a detailed discussion and overview). **We emphasize that DR has not yet been measured with two independent methods in the same object, which is highly desirable as a check.** As the outer convection zone is thought to be the site where the stellar dynamo ought to operate, DR is crucial to understand the theory of magnetic field generation in stars and, thus ultimately, stellar activity.

During the transit of a planet in front of its host star, different sections of the rotating stellar surface are consecutively covered, leading to distortions in the spectral line profile. Even if the planet-induced line distortion is not resolved, the transit still shows up as an apparent, anomalous radial-velocity (RV) shift, known as the Rossiter-McLaughlin effect. Measurements of the latter allow to determine the projected stellar rotation velocity, $v\sin(i)$, and the sky-projected angle between the stellar spin axis and the planetary orbit normal, usually referred to as the "spin-orbit misalignment", λ.

In Fig. 1 B we show the Rossiter-McLaughlin effect as determined in WASP-7 by Albrecht et al. 2012 (ApJ, 744). Clearly, the Rossiter-McLaughlin RV curve is markedly asymmetric consisting only of a time-variable blue shift; a detailed analysis by these authors does indeed reveal a spin-orbit misalignment angle of $\lambda = 86^\circ \pm 6^\circ$ and an orbital inclination of 87.2° (see Fig. 1 A); furthermore, the stellar inclination is likely $\approx 90^\circ$.

Due to the unusual geometry of WASP-7, the planet "scans" the stellar surface from lowest to highest latitudes, traversing almost the entire range of surface differential rotation and limb-darkening. Although F5V stars like WASP-7 are predicted to show high levels of DR (e.g., Augustson et al. 2012, ApJ, 756), DR measurements can hardly be obtained from the Rossiter-McLaughlin effect alone, since it is impossible to disentangle the influences of limb-darkening and DR on the spectral line-profile based solely on RV measurements (Albrecht et al. 2012). This ambiguity can, however, be broken by analyzing the spectral signatures directly by means of an average line profile—a technique known as "line-profile tomography". While the strength of the planet-induced spectral distortion mainly depends on the amount of blocked light, and therefore on limb-darkening, its location in wavelength space is entirely determined by the rotation profile of the stellar surface (cf., Fig. 1 D,E). As strength and location can be determined separately in the line profile, limb-darkening and DR can also be analyzed *independently* using this technique.

While line-profile tomography has already been successfully applied to three planetary systems, namely, WASP-33, HD 189733, and CoRoT-11 (Collier Cameron et al. 2010, MNRAS, 407 and MNRAS, 403; Gandolfi et al. 2012, A&A, 543), a similar analysis is not reliably possible with the data analyzed by Albrecht et al. (2012), because they were taken with an iodine cell.

B – Immediate Objective: We propose to obtain high-resolution, low-noise transit spectroscopy of the bright, southern ($\delta = -39^\circ$) exoplanetary system WASP-7 using UVES. **Based on the anticipated series of spectra, we will measure the degree of surface differential rotation in WASP-7 using two independent techniques: (a) line-profile tomography, and (b) the "Fourier technique".** Our measurement would thus for the first time allow to compare two complementary DR measurements in the same object. The combination of its special geometry, its long transit duration ($\approx$ 4 h), its fast rotating host-star ($v\sin(i) \approx 17$ km/s), and its brightness (V= 9.5 mag) make WASP-7 an almost perfect target to study surface differential rotation via line-profile tomography.

To successfully apply line-profile tomography, high spectral resolution and high signal-to-noise ratios (SNR) are indispensable. We used the UVES exposure time calculator to estimate that, for the spectral type of WASP-7 (F5V), a SNR of 120 – 160 per spectral bin (0.03 Å) is obtained nearly across the entire wavelength range covered in the "dic-2 437+760" setting with a 300 s exposure at a spectral resolution of 80 000, assuming an airmass of 1.6 and a seeing of 1″. Given a transit duration of 4.1 h and assuming an overhead of 100 s per exposure, we estimate that 37 transit spectra can be obtained. Additionally, our proposed schedule (see Sect. 8) allows to obtain 9 spectra before and after the transit, which are crucial to obtain an undistorted "reference line-profile" to be compared with the in-transit profile and to be able to apply the Fourier technique (this is possible only for the non-transit spectra).

7. Description of the proposed programme and attachments

Description of the proposed programme (continued)

As a "proof of concept", we, first, applied the method to transit spectroscopy of WASP-33 previously obtained by our group using CAFE at the 2.2 m on Calar Alto, and, second, carried out simulations to assess the feasibility of our proposal under realistic conditions in WASP-7.

In Dec. 2011, we obtained 24 spectra of WASP-33 using CAFE, of which 12 were obtained during transit. The mean SNR of these spectra is 60 at a spectral resolution of $\approx 60\,000$. We now defined 60 spectral chunks with an individual length between 10 and 20 Å, normalized these spectral chunks, and fitted a spectral model based on a synthetic line list. Based on this model, we determined the broadening function using the least-squares deconvolution technique. In Fig. 1 C, we show the average residual line-profile, i.e., the summed deviation from the mean profile, obtained for our CAFE data. The shown map is similar to that presented by Collier Cameron et al. 2010 (their Fig. 4) showing pronounced structures running from negative to positive radial velocities caused by the pulsations of the host star. *Only during transit,* there is another structure moving in the reverse direction—this is the unambiguous signature of the retrogradely orbiting planet.

As we have not yet obtained suitable data for our actual target WASP-7 in public archives, we calculated synthetic spectra based on ATLAS model atmospheres, applied a SNR of 120, and included the effect of WASP-7b on the line profiles considering various levels of differential rotation. We then adopted the same procedure as for WASP-33. In total, we used a spectral interval of 2800 Å divided into 140 individual chunks, 37 transit spectra, and 20 out-of-transit spectra to obtain the unaffected line profile. After subtracting the broadening function determined from the out-of-transit observations, the signal of the planet in each transit observation becomes visible (see Fig. 1 D). The position and strength of the signal in the broadening function gives the radial velocity and brightness of the stellar surface below the planet independently (Fig. 1 E).

For a rigidly rotating stellar surface, the planet would show up as straight line in the line-profile map, because the planetary path across the star is a straight line and the radial velocity of the stellar surface depends only on the distance from the rotation axis. For a differentially rotating star the RV shift depends on stellar latitude and consequently the RV shift shows a DR dependent curvature (Fig. 1 D,E). The effect is strongest for highly oblique orbits ($\lambda \gg 0°$) such as WASP-7b and it is this curvature in the RV shift, which allows to measure the level of DR.

In our simulations, we assumed a solar-like DR law and a value of 0.5 for $\alpha = (P_{\rm pole} - P_{\rm eq})/P_{\rm pole}$, which is not unrealistic as shown observationally by Ammler-von Eiff and Reiners 2012 (A&A, 542) and theoretically, e.g., by Augustson et al. 2012 (ApJ, 756). The curvature effect and hence DR is clearly seen in our simulations (Fig. 1 D,E). According to our modeling, we will be able to measure DR as low as $\alpha = 0.1$; in the shown example, we could recover the input of $\alpha = 0.5$ quite accurately obtaining $\alpha = 0.48 \pm 0.04$. Similarly, the limb-darkening coefficient could be reproduced with an uncertainty of about 30%. Our simulations thus clearly demonstrate that our proposed program is feasible and that WASP-7 is the ideal target to measure DR using a planet for the first time.

Attachments (Figures)

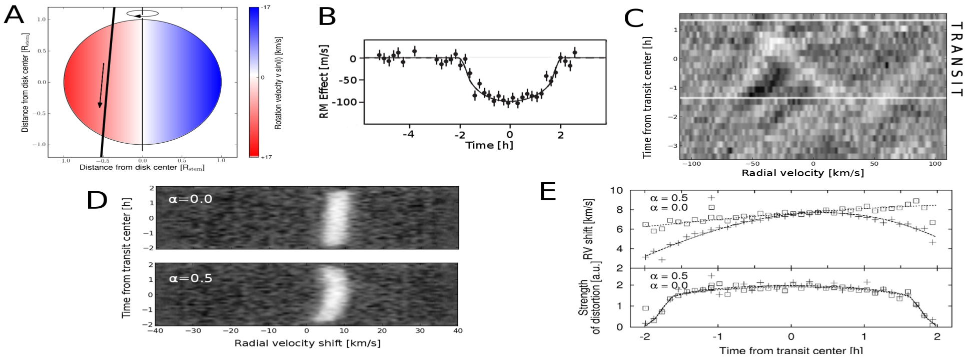

Fig.1: A) Transit geometry of WASP-7. **B)** Rossiter-McLaughlin effect in WASP-7 (from Albrecht el al. 2012). **C)** Residual line-profile map of WASP-33 showing the planetary signal moving from positive to negative RVs. **D)** Simulated line-profile map of WASP-7 with no differential rotation (top) and $\alpha = 0.5$ (bottom). **E)** RV shift (top) and strength (bottom) of the distortion determined through Gaussian fit.

8. Justification of requested observing time and observing conditions

Lunar Phase Justification: No lunar phase restrictions

Time Justification: (including seeing overhead) WASP-7 has a relatively long orbital period of 4.95 d and, consequently, a transit duration of 3.77 h. We need to cover the entire transit plus 1 h time before and after the transit, which is required to obtain a "reference line-profile" without the planetary signal. This reference profile will be compared with the in-transit line profiles and used to study DR using the Fourier technique. Therefore, our total time request amounts to 6.1 h. The long transit duration and nearly integer orbital period of ≈ 5 d limit the number of nights during which our proposed observations can be scheduled. In fact, we found that only during the night between 31 Aug. - 2. Sept. 2013, perfect conditions for our observations are encountered: During this night, the transit lasts from 02:02 UT to 05:49 UT and WASP-7 culminates at 02:50 UT at an altitude of 75°. Therefore, WASP-7 can be observed at airmass < 2 during the entire observation (transit plus 1 h before and after). We checked that also the Moon distance (≈ 55°) fits the requirements. In summary, the night 31 Aug. - 2. Sept, 2013 is perfectly suited for our measurements.

8a. Telescope Justification:

To successfully measure DR via line-profile tomography, we require a series of high-quality spectra (SNR ≥ 100, spectral resolution $\geq 60\,000$) taken at the shortest possible temporal cadence—the latter minimizes the effect of "phase-smearing" and increases our chances to measure DR. With UVES installed at UT2 (Kueyen), a temporal sampling of ≈ 400 s can be reached, corresponding to 37 transit spectra. Furthermore, the target is perfectly located in the night sky to be observed from Paranal.

8b. Observing Mode Justification (visitor or service):

Due to the time-critical nature of our proposed observations, we prefer visitor mode for our program and are prepared to send an experienced observer to Paranal. In our experience, the success of the proposed program can be best ensured when an actual observer is present, since time-dependent local sky conditions may need to be taken into account, decisions about possible changes in slit width or exposure time during the run may have to be taken depending on the quality of the obtained spectra. However, if the TAC deems service mode appropriate, this will also be acceptable.

8c. Calibration Request:

Special Calibration - Adopt a special calibration

9. Report on the use of ESO facilities during the last 2 years

The COIs have obtained UVES data during the last two years: Transit spectroscopy of HD 189733 (S. Czesla: visiting astronomer, U. Wolter: PI, program ID 089.D-0701(A), UVES 30-06-2012);
“The age of the CoRoT-2 exoplanetary system” (U. Wolter: PI, program ID 088.D-0383(A)), Service mode 2011-12, not completed.

9a. ESO Archive - Are the data requested by this proposal in the ESO Archive (http://archive.eso.org)? If so, explain the need for new data.

We verified that the ESO archive does not contain any data, which could compete with our proposed observations.

9b. GTO/Public Survey Duplications:

10. Applicant's publications related to the subject of this application during the last 2 years

Czesla, S.; Schröter, S.; Wolter, U.; von Essen, C.; Huber, K. F.; Schmitt, J. H. M. M.; Reichart, D. E.; Moore, J. P, A&A, 539, 150: “The extended chromosphere of CoRoT-2A. Discovery and analysis of the chromospheric Rossiter-McLaughlin effect”

Schröter, S.; Czesla, S.; Wolter, U.; Müller, H. M.; Huber, K. F.; Schmitt, J.H. M. M.: “The corona and companion of CoRoT-2a. Insights from X-rays and optical spectroscopy”, A&A, 532, 3

11. List of targets proposed in this programme

Run	Target/Field	α(J2000)	δ(J2000)	ToT	Mag.	Diam.	Additional info	Reference star
A	WASP-7	20 44 10.219	-39 13 30.8	6.1	9.5			

Target Notes: A note about the targets and/or strategy of selecting the targets during the run. For APEX runs please remember to specify the PWV limits for each target under 'Additional info' in the table above.

12. Scheduling requirements

This proposal involves time-critical observations, or observations to be performed at specific time intervals.

12. Scheduling requirements contd...

4. Specific date(s) for time critical observations:

Run	**from**	**to**	**reason**
A	31-aug-13	01-sep-13	In this night, the entire (3.77 h) transit of WASP-7 including sufficient pre- and post-transit time (2×1 h) can be observed at an airmass < 2. The transit lasts from 02:02 UT to 05:49 UT (22:02 to 01:49 local time in Chile).

13. Instrument configuration

Period	Instrument	Run ID	Parameter	Value or list
91	UVES	A	DIC-2	Standard setting: 437+760

Bibliography

[1] Albrecht, S. et al. “Obliquities of Hot Jupiter Host Stars: Evidence for Tidal Interactions and Primordial Misalignments”. In: ApJ 757, 18 (Sept. 2012), p. 18. DOI: 10.1088/0004-637X/757/1/18. arXiv: 1206.6105 [astro-ph.SR].

[2] Bakos, G., Hartman, J. D., et al. “HAT-P-34b-HAT-P-37b: Four Transiting Planets More Massive than Jupiter Orbiting Moderately Bright Stars”. In: AJ 144, 19 (July 2012), p. 19. DOI: 10.1088/0004-6256/144/1/19. arXiv: 1201.0659 [astro-ph.EP].

[3] Bakos, G., Kovács, G., et al. “HD 147506b: A Supermassive Planet in an Eccentric Orbit Transiting a Bright Star”. In: ApJ 670 (Nov. 2007), pp. 826–832. DOI: 10.1086/521866. arXiv: 0705.0126.

[4] Butler, R. P. et al. “Attaining Doppler Precision of 3 M s-1”. In: PASP 108 (June 1996), p. 500. DOI: 10.1086/133755.

[5] C., J. and Brown, C. I. J. D. *Inverse problems in astronomy - a guide to inversion strategies for remotely sensed data*. Bristol: A. Hilger, 1986. ISBN: 978-0-852-74369-0.

[6] CAHA. *CAFE spectrograph*. URL: http://www.caha.es/CAHA/Instruments/CAFE/index.html.

[7] CAHA. *Centro Astronomico Hispano-Aleman*. URL: http://www.caha.es.

[8] Christian, D. J. et al. “The SuperWASP wide-field exoplanetary transit survey: candidates from fields 23 h < RA < 03 h”. In: MNRAS 372 (Nov. 2006), pp. 1117–1128. DOI: 10.1111/j.1365-2966.2006.10913.x.

[9] Collier Cameron, A., Bruce, V. A., et al. “Line-profile tomography of exoplanet transits - I. The Doppler shadow of HD 189733b”. In: MNRAS 403 (Mar. 2010), pp. 151–158. DOI: 10.1111/j.1365-2966.2009.16131.x. arXiv: 0911.5361 [astro-ph.SR].

[10] Collier Cameron, A., Guenther, E., et al. “Line-profile tomography of exoplanet transits - II. A gas-giant planet transiting a rapidly rotating A5 star”. In: MNRAS 407 (Sept. 2010), pp. 507–514. DOI: 10.1111/j.1365-2966.2010.16922.x. arXiv: 1004.4551 [astro-ph.EP].

[11] Czesla, S. et al. *PyAstronomy*. URL: https://github.com/sczesla/PyAstronomy.

[12] Davis, M., Geller, M. J., and Huchra, J. “The local mean mass density of the universe - New methods for studying galaxy clustering”. In: ApJ 221 (Apr. 1978), pp. 1–18. DOI: 10.1086/156000.

[14] Eastman, J. *Time conversion utilities*. URL: http://astroutils.astronomy.ohio-state.edu/time/.

[15] Eastman, J., Siverd, R., and Gaudi, B. S. “Achieving Better Than 1 Minute Accuracy in the Heliocentric and Barycentric Julian Dates”. In: PASP 122 (Aug. 2010), pp. 935–946. DOI: 10.1086/655938. arXiv: 1005.4415 [astro-ph.IM].

[16] ESO. *European Southern Observatory*. URL: http://www.eso.org/sci.

[17] ESO. *UVES spectrograph*. URL: http://www.eso.org/sci/facilities/paranal/instruments/uves/overview.html.

[18] Gandolfi, D. et al. “Doppler tomography of transiting exoplanets: a prograde, low-inclined orbit for the hot Jupiter CoRoT-11b”. In: A&A 543, L5 (July 2012), p. L5. DOI: 10.1051/0004-6361/201219533. arXiv: 1206.4037 [astro-ph.EP].

[19] Giménez, A. “Equations for the Analysis of the Rossiter-MCLaughlin Effect in Extrasolar Planetary Transits”. In: ApJ 650 (Oct. 2006), pp. 408–413. DOI: 10.1086/507021.

[20] Gray, D. F. *SPECTRUM*. URL: http://www.appstate.edu/~grayro/spectrum/spectrum.html.

[21] Gray, D. F. *The Observation And Analysis Of Stellar Photospheres*. 3. Cambridge: Cambridge University Press, 2005. ISBN: 978-0-521-85186-2.

[22] H., G. and Golub, L. C. F. V. *Matrix Computations*. London: JHU Press, 2012. ISBN: 978-1-421-40859-0.

[23] H., W. et al. *Numerical Recipes 3rd Edition - The Art of Scientific Computing*. 3. Cambridge: Cambridge University Press, 2007. ISBN: 978-0-521-88068-8.

[24] HATNet. *Hungarian Automated Telescope Network*. URL: https://www.cfa.harvard.edu/~gbakos/HAT.

[25] Hauschildt, P. H. and Baron, E. *PHOENIX*. URL: http://www.hs.uni-hamburg.de/EN/For/ThA/phoenix/index.html.

[26] Hirano, T., Suto, Y., Taruya, A., et al. "Analytic Description of the Rossiter-Mclaughlin Effect for Transiting Exoplanets: Cross-Correlation Method and Comparison with Simulated Data". In: ApJ 709 (Jan. 2010), pp. 458–469. DOI: 10.1088/0004-637X/709/1/458. arXiv: 0910.2365 [astro-ph.EP].

[27] Hirano, T., Suto, Y., Winn, J. N., et al. "Improved Modeling of the Rossiter-McLaughlin Effect for Transiting Exoplanets". In: ApJ 742, 69 (Dec. 2011), p. 69. DOI: 10.1088/0004-637X/742/2/69. arXiv: 1108.4430 [astro-ph.EP].

[29] KECK. *HIRES spectrograph*. URL: http://www2.keck.hawaii.edu/inst/hires/.

[32] Kurucz, R. L. "Model atmospheres for G, F, A, B, and O stars". In: ApJS 40 (May 1979), pp. 1–340. DOI: 10.1086/190589.

[33] Lewis, N. K. et al. "Orbital Phase Variations of the Eccentric Giant Planet HAT-P-2b". In: ApJ 766, 95 (Apr. 2013), p. 95. DOI: 10.1088/0004-637X/766/2/95. arXiv: 1302.5084 [astro-ph.EP].

[34] Lewis, N. et al. "Analysis of HAT-P-2b Warm Spitzer Full Orbit Light Curve". In: *American Astronomical Society Meeting Abstracts #218*. May 2011, p. 218.04.

[35] Loeillet, B. et al. "Refined parameters and spectroscopic transit of the super-massive planet HD 147506b". In: A&A 481 (Apr. 2008), pp. 529–533. DOI: 10.1051/0004-6361:20078167. arXiv: 0707.0679.

[36] Mandel, K. and Agol, E. "Analytic Light Curves for Planetary Transit Searches". In: ApJ 580 (Dec. 2002), pp. L171–L175. DOI: 10.1086/345520. eprint: arXiv:astro-ph/0210099.

[37] Mayor, M. and Queloz, D. "A Jupiter-mass companion to a solar-type star". In: Nature 378 (Nov. 1995), pp. 355–359. DOI: 10.1038/378355a0.

[38] McLaughlin, D. B. "Some results of a spectrographic study of the Algol system." In: ApJ 60 (July 1924), pp. 22–31. DOI: 10.1086/142826.

[39] Murray, C. D. and Correia, A. C. "Keplerian Orbits and Dynamics of Exoplanets". In: *Exoplanets, edited by S. Seager. Tucson, AZ: University of Arizona Press, 2011, 526 pp. ISBN 978-0-8165-2945-2., p.15-23*. University of Arizona Press, 2011, pp. 15–23.

[40] NASA. *KEPLER satellite*. URL: http://kepler.nasa.gov/.

[41] Nutzman, P. A., Fabrycky, D. C., and Fortney, J. J. "Using Star Spots to Measure the Spin-orbit Alignment of Transiting Planets". In: ApJ 740, L10 (Oct. 2011), p. L10. DOI: 10.1088/2041-8205/740/1/L10. arXiv: 1107.2106 [astro-ph.EP].

[42] OHP. *Observatoire de Haute-Provence*. URL: http://www.obs-hp.fr.

[43] OHP. *SOPHIE spectrograph*. URL: http://www.obs-hp.fr/guide/sophie/sophie-eng.shtml.

[44] Ohta, Y., Taruya, A., and Suto, Y. "The Rossiter-McLaughlin Effect and Analytic Radial Velocity Curves for Transiting Extrasolar Planetary Systems". In: ApJ 622 (Apr. 2005), pp. 1118–1135. DOI: 10.1086/428344. eprint: arXiv:astro-ph/0410499.

[45] Pál, A. et al. "Refined stellar, orbital and planetary parameters of the eccentric HAT-P-2 planetary system". In: MNRAS 401 (Feb. 2010), pp. 2665–2674. DOI: 10.1111/j.1365-2966.2009.15849.x. arXiv: 0908.1705 [astro-ph.EP].

[46] Perryman, M. "Resource Letter Exo-1: Exoplanets". In: *ArXiv e-prints* (Nov. 2013). arXiv: 1311.2521 [astro-ph.EP].

[48] Piskunov, N. E. and Valenti, J. A. "New algorithms for reducing cross-dispersed echelle spectra". In: A&A 385 (Apr. 2002), pp. 1095–1106. DOI: 10.1051/0004-6361:20020175.

[49] Queloz, D. et al. "Detection of a spectroscopic transit by the planet orbiting the star HD209458". In: A&A 359 (July 2000), pp. L13–L17. eprint: astro-ph/0006213.

[50] R. Heller. *Holt-Rossiter-McLaughlin Encyclopaedia*. URL: http://www.physics.mcmaster.ca/~rheller/content/main_HRM.html.

[51] Rosner, B. "Percentage Points for a Generalized ESD Many-Outlier Procedure". In: Technometrics 25 (May 1983), pp. 162–172. DOI: 10.1080/00401706.1983.10487848. eprint: 1004.4551.

[52] Rossiter, R. A. "On the detection of an effect of rotation during eclipse in the velocity of the brigher component of beta Lyrae, and on the constancy of velocity of this system." In: ApJ 60 (July 1924), pp. 15–21. DOI: 10.1086/142825.

[53] Hearnshaw, J. B. and Scarfe, C. D., eds. *Determination of Broadening Functions Using the Singular-Value Decomposition (SVD) Technique.* Vol. 185. Astronomical Society of the Pacific Conference Series. 1999, p. 82. eprint: astro-ph/9807327.

[55] Sanchis-Ojeda, R. et al. “Starspots and Spin-orbit Alignment in the WASP-4 Exoplanetary System”. In: ApJ 733, 127 (June 2011), p. 127. DOI: 10.1088/0004-637X/733/2/127. arXiv: 1103.4859 [astro-ph.EP].

[56] Schlaufman, K. C. “Evidence of Possible Spin-orbit Misalignment Along the Line of Sight in Transiting Exoplanet Systems”. In: ApJ 719 (Aug. 2010), pp. 602–611. DOI: 10.1088/0004-637X/719/1/602. arXiv: 1006.2851 [astro-ph.EP].

[57] Simkin, S. M. “Measurements of Velocity Dispersions and Doppler Shifts from Digitized Optical Spectra”. In: A&A 31 (Mar. 1974), p. 129.

[58] Smith, A. M. et al. “Thermal emission from WASP-33b, the hottest known planet”. In: MNRAS 416 (Sept. 2011), pp. 2096–2101. DOI: 10.1111/j.1365-2966.2011.19187.x. arXiv: 1101.2432 [astro-ph.EP].

[59] SuperWASP. *Wide Angle Search For Planets.* URL: http://www.superwasp.org.

[60] Tonry, J. and Davis, M. “A survey of galaxy redshifts. I - Data reduction techniques”. In: AJ 84 (Oct. 1979), pp. 1511–1525. DOI: 10.1086/112569.

[61] VALD. *Vienna Atomic Line Data-Base.* URL: http://www.astro.uu.se/~vald/php/vald.php.

[62] Valenti, J. A. and Piskunov, N. “Spectroscopy made easy: A new tool for fitting observations with synthetic spectra.” In: A&AS 118 (Sept. 1996), pp. 595–603.

[63] Vogt, S. S. and Penrod, G. D. “Doppler Imaging of spotted stars - Application to the RS Canum Venaticorum star HR 1099”. In: PASP 95 (Sept. 1983), pp. 565–576. DOI: 10.1086/131208.

[64] Winn, J. N., Fabrycky, D., et al. “Hot Stars with Hot Jupiters Have High Obliquities”. In: ApJ 718 (Aug. 2010), pp. L145–L149. DOI: 10.1088/2041-8205/718/2/L145. arXiv: 1006.4161 [astro-ph.EP].

[65] Winn, J. N., Holman, M. J., et al. “The Transit Light Curve Project. IX. Evidence for a Smaller Radius of the Exoplanet XO-3b”. In: ApJ 683 (Aug. 2008), pp. 1076–1084. DOI: 10.1086/589737. arXiv: 0804.4475.

[66] Winn, J. N., Johnson, J. A., Fabrycky, D., et al. “On the Spin-Orbit Misalignment of the XO-3 Exoplanetary System”. In: ApJ 700 (July 2009), pp. 302–308. DOI: `10.1088/0004-637X/700/1/302`. arXiv: `0902.3461 [astro-ph.EP]`.

[67] Winn, J. N., Johnson, J. A., Peek, K. M., et al. “Spin-Orbit Alignment for the Eccentric Exoplanet HD 147506b”. In: ApJ 665 (Aug. 2007), pp. L167–L170. DOI: `10.1086/521362`. arXiv: `0707.0503`.

[68] Zucker, S. “Cross-correlation and maximum-likelihood analysis: a new approach to combining cross-correlation functions”. In: MNRAS 342 (July 2003), pp. 1291–1298. DOI: `10.1046/j.1365-8711.2003.06633.x`. eprint: `astro-ph/0303426`.

Further Reading

[13] Dekker, H. et al. “Design, construction, and performance of UVES, the echelle spectrograph for the UT2 Kueyen Telescope at the ESO Paranal Observatory”. In: *Optical and IR Telescope Instrumentation and Detectors*. Ed. by Iye, M. and Moorwood, A. F. Vol. 4008. Society of Photo-Optical Instrumentation Engineers (SPIE) Conference Series. Aug. 2000, pp. 534–545.

[28] Huber, K. F. et al. “Planetary eclipse mapping of CoRoT-2a. Evolution, differential rotation, and spot migration”. In: A&A 514, A39 (May 2010), A39. DOI: `10.1051/0004-6361/200913914`. arXiv: `1002.4113 [astro-ph.SR]`.

[30] Kupka, F. G. et al. “VALD-2 – The New Vienna Atomic Line Database”. In: *Baltic Astronomy* 9 (2000), pp. 590–594.

[31] Kupka, F. et al. “VALD-2: Progress of the Vienna Atomic Line Data Base”. In: A&AS 138 (July 1999), pp. 119–133. DOI: `10.1051/aas:1999267`.

[47] Piskunov, N. E., Kupka, F., et al. “VALD: The Vienna Atomic Line Data Base.” In: A&AS 112 (Sept. 1995), p. 525.

[54] Ryabchikova, T. A. et al. “The Vienna Atomic Line Database : Present State and Future Development”. In: *Baltic Astronomy* 6 (Mar. 1997), pp. 244–247.